Title

Apical-Basal Polarity Signaling Components, Lgl1 and aPKCs, Control Glutamatergic Synapse Number and Function

Authors

Scott, John

Thakar, Sonal

Mao, Ye

et al.

Publication Date

2019-10-01

DOI

10.1016/j.isci.2019.09.005

iScience

CellPress

Article

Apical-Basal Polarity Signaling Components, Lgl1 and aPKCs, Control Glutamatergic Synapse Number and Function

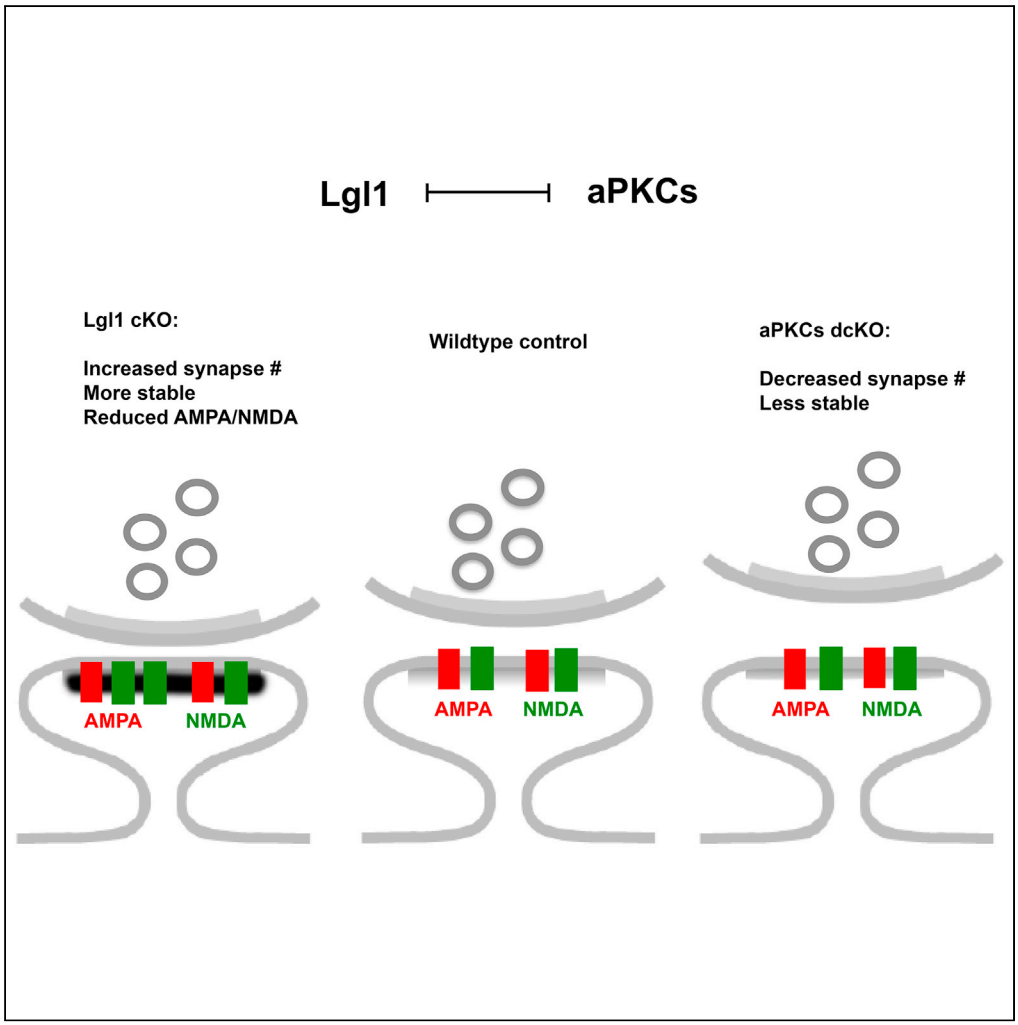

John Scott, Sonal Thakar, Ye Mao, ..., Sourav Ghosh, Valeri Vasioukhin, Yimin Zou

yzou@ucsd.edu

HIGHLIGHTS

Lgl1 regulates glutamatergic synapse numbers by inhibiting aPKC

Lgl1 cKO leads to reduced AMPA/NMDA ratio in development and adulthood

Lgl1 conditional knockout impairs novel object cognition and social interaction

Social interaction deficits can be rescued by NMDA receptor blockade

Scott et al., iScience *20*, 25–41
October 25, 2019
https://doi.org/10.1016/j.isci.2019.09.005

iScience

CellPress

Article

Apical-Basal Polarity Signaling Components, Lgl1 and aPKCs, Control Glutamatergic Synapse Number and Function

John Scott,[1] Sonal Thakar,[1] Ye Mao,[4] Huaping Qin,[1] Helen Hejran,[1] Su-Yee Lee,[1] Ting Yu,[1] Olga Klezovitch,[2] Hongqiang Cheng,[4] Yongxin Mu,[4] Sourav Ghosh,[3] Valeri Vasioukhin,[2] and Yimin Zou[1,*]

SUMMARY

Normal synapse formation is fundamental to brain function. We show here that an apical-basal polarity (A-BP) protein, Lgl1, is present in the postsynaptic density and negatively regulates glutamatergic synapse numbers by antagonizing the atypical protein kinase Cs (aPKCs). A planar cell polarity protein, Vangl2, which inhibits synapse formation, was decreased in synaptosome fractions of cultured cortical neurons from *Lgl1* knockout embryos. Conditional knockout of *Lgl1* in pyramidal neurons led to reduction of AMPA/NMDA ratio and impaired plasticity. *Lgl1* is frequently deleted in Smith-Magenis syndrome (SMS). Lgl1 conditional knockout led to increased locomotion, impaired novel object recognition and social interaction. *Lgl1+/−* animals also showed increased synapse numbers, defects in open field and social interaction, as well as stereotyped repetitive behavior. Social interaction in *Lgl1+/−* could be rescued by NMDA antagonists. Our findings reveal a role of apical-basal polarity proteins in glutamatergic synapse development and function and also suggest a potential treatment for SMS patients with *Lgl1* deletion.

INTRODUCTION

Glutamatergic synapses are the major class of excitatory synapses in the mammalian central nervous system (Collingridge et al., 1983; Monaghan et al., 1989; Watkins and Evans, 1981). Normal development and plasticity of glutamatergic synapses are essential to the emergence of normal behavioral functions, the disruption of which causes various neurological and neuropsychiatric disorders. A recent study showed that components of planar cell polarity (PCP) signaling pathway are key regulators of glutamatergic synapse formation (Thakar et al., 2017). Celsr3 is essential for glutamatergic synapse formation, whereas Vangl2 negatively regulates glutamatergic synapse formation. Therefore, PCP signaling components can both positively and negatively regulate glutamatergic synapse numbers.

Lethal giant larvae (Lgl1) is a key component of the highly conserved apical-basal polarity signaling pathway, which polarizes epithelial cells along the apical and basolateral axis (Karner et al., 2006). Lgl1 forms the basolateral complexes with Scribble and Discs Large (Dlg) and mutually excludes and antagonizes the function of the apical complex, the aPKC/Par3/Par6 complex. Lgl1 has been implicated in polarized exocytosis and is essential for establishing or maintaining apical-basal polarity (Betschinger et al., 2003; Georgiou et al., 2008; Macara, 2004; Yamanaka et al., 2003, 2006). Dlg homologs are important postsynaptic scaffold proteins, called *MAGUKs* (Zhu et al., 2016). MAGUK proteins play essential roles in postsynaptic density organization and glutamate receptor trafficking and clustering. In addition, Lgl1 has been shown to associate and co-traffic with FMRP (Zarnescu et al., 2005), a translational regulator of many synaptic components. Apical-basal and planar polarity pathways are known to interact with each other. For example, apical-basal polarity signaling has been recently shown to regulate the location of PCP signaling (Chuykin et al., 2018).

Here we report that conditional knockout of *Lgl1* from postnatal day 7 (P7) in hippocampal pyramidal neurons, before the peak of glutamatergic synapse formation, resulted in increased glutamatergic synapse density. In *aPKC* double conditional knockout (KO) (dcKO), glutamatergic synapse numbers were initially normal (at P14) but were reduced in adulthood. *Triple conditional KO (tcKO)* of *Lgl1* and *aPKCs* rescued the defects of synapse numbers in *Lgl1 cKO*. In the synaptosome fraction of cultured *Lgl1−/−* neurons Vangl2 was found decreased. *Lgl1 cKO* and *aPKC dcKO* led to opposite changes in ultrastructure, with

[1]Neurobiology Section, Biological Sciences Division, University of California, San Diego, La Jolla, CA 92093, USA

[2]Division of Human Biology, Fred Hutchinson Cancer Research Center, Seattle, WA 98109, USA

[3]Department of Neurology, Yale University, New Haven, CT 06511, USA

[4]Department of Medicine, University of California, San Diego, La Jolla, CA 92093, USA

*Correspondence: yzou@ucsd.edu

https://doi.org/10.1016/j.isci.2019.09.005

loss of Lgl1 leading to a larger postsynaptic density and smaller synaptic cleft. *Lgl1 cKO* also showed reduced AMPA/NMDA receptor ratio. Deleting Lgl1 in adulthood also led to increased synapse numbers and a much greater reduction of AMPA/NMDA receptor ratio, as well as deficit in long-term potentiation. These results suggest that Lgl1 regulates glutamate receptor trafficking, potentially through its binding partners, the MAGUK proteins. Therefore, together with PCP signaling, apical-basal signaling also has a profound influence on synapse formation, forming another layer of regulation, potentially allowing additional regulatory inputs.

Lgl1 is frequently deleted in a chromosome 17 p11.2 microdeletion disorder, called Smith-Magenis syndrome (SMS) (Smith et al., 1986). SMS is a *de novo* genetic disorder arising very early in embryonic development through homologous recombination (Chen et al., 1997). A deletion interval of 3.5 Mb occurs in approximately 70% of patients (Gropman et al., 2007). Individuals with the deletion are frequently diagnosed with autism spectrum disorders (ASDs), attention-deficit/hyperactivity disorder, obsessive-compulsive disorder (OCD), or other behavioral disorders (Dykens et al., 1997; Dykens and Smith, 1998; Laje et al., 2010; Martin et al., 2006; Smith et al., 1998). Symptoms vary between individuals despite common deletions (Edelman et al., 2007; Potocki et al., 2003), and multiple genes likely contribute to the syndrome (Girirajan et al., 2006). Recent work has implicated *Rai1* in non-ASD symptoms of SMS (Huang et al., 2016). The locus for *Lgl1* lies within a refined consensus deletion site of ~950 kb for SMS that has been reported in genetic studies of patients carrying the chromosomal deletion (Vlangos et al., 2003). Fluorescence *in situ* hybridization probes targeting the sequence for the human homolog of *Lgl1* fail to hybridize with one of the copies of chromosome 17 in patients with SMS (Koyama et al., 1996). The functional role of *Lgl1* in SMS has not been reported.

We found that *Lgl1* conditional KO in excitatory neurons from early postnatal stages (P7) resulted in behavioral deficits in adulthood, such as hyperactivity, cognitive impairment, and social interaction defects. We found that *Lgl1+/−* animals also had higher synapse numbers and showed impaired social interaction and increased stereotyped repetitive behaviors. Patients with SMS show either seizures or abnormal electroencephalography (EEG) without overt seizure (Chen et al., 1996; Greenberg et al., 1996). We found that *Lgl1+/−* animals have lower seizure threshold. Because our electrophysiological and biochemical results suggest higher NMDA activity in *Lgl1* mutants, we tested whether NMDA blockers could rescue any of the behavioral deficits and found that low-dose ketamine, MK801, and memantine could rescue the social interaction deficit of *Lgl+/−* animals. Therefore, apical-basal cell polarity signaling components are also essential for normal synaptic function and the loss of their function may cause neuropsychiatric disorders; these NMDA blockers may help alleviate certain behavioral symptoms of SMS patients with *Lgl1* deletion.

RESULTS

Increased Glutamatergic Synapse Numbers and Reduced AMPA/NMDA Ratio in *Lgl1* Conditional Knockout *In Vivo*

Glutamatergic synapse formation starts shortly after birth. Lgl1 has roles in earlier stages of development, including neurogenesis. To avoid early developmental defects, we conditionally knocked out *Lgl1* in hippocampal pyramidal neurons from postnatal day 7 (P7) using an inducible *Cre* line, *SLICK-H* (Figures S1A–S1C) (Heimer-McGinn and Young, 2011). Tamoxifen was injected intraperitoneally on P7 and postnatal day 8 (P8) and animals were euthanized and perfused on postnatual day 14 (P14) for electron microscopy. We counted asymmetric and symmetric synapses in the stratum radiatum. Images were taken 150–200 μm from the CA1 cell body layer in brain slices. We observed a 28.7% increase in the density of asymmetric (excitatory) synapse that are formed on dendritic spines (Figure 1A). Axo-dendritic synapses show no change in density. No significant change was observed in symmetric (inhibitory) synapse density in these slices.

To determine whether the increased synapses persist, we fixed slices from 8-week old adult mice that had tamoxifen injection at P7 and P8. In these animals, we observed an increase of 31.8% in asymmetric synapse density 150–200 μm from the CA1 cell body layer (Figure 1B). In contrast to juvenile animals, adult animals show a statistically significant 25.5% increase in density of symmetric synapses in the region 50 μm from the CA1 cell layer. The delay in the increase of symmetric synapses suggests that it is not directly caused by the loss of function of *Lgl1*, but possibly by a homeostatic response of the hippocampal circuitry. The number of asymmetric synapses in the region 50 μm from the CA1 cell layer also shows an increase (Figures S1D and S1E).

To assess the function of the increased synapses, we recorded miniature excitatory postsynaptic currents (mEPSCs) and miniature inhibitory postsynaptic currents (mIPSCs) from acute brain slices from P14 and P15

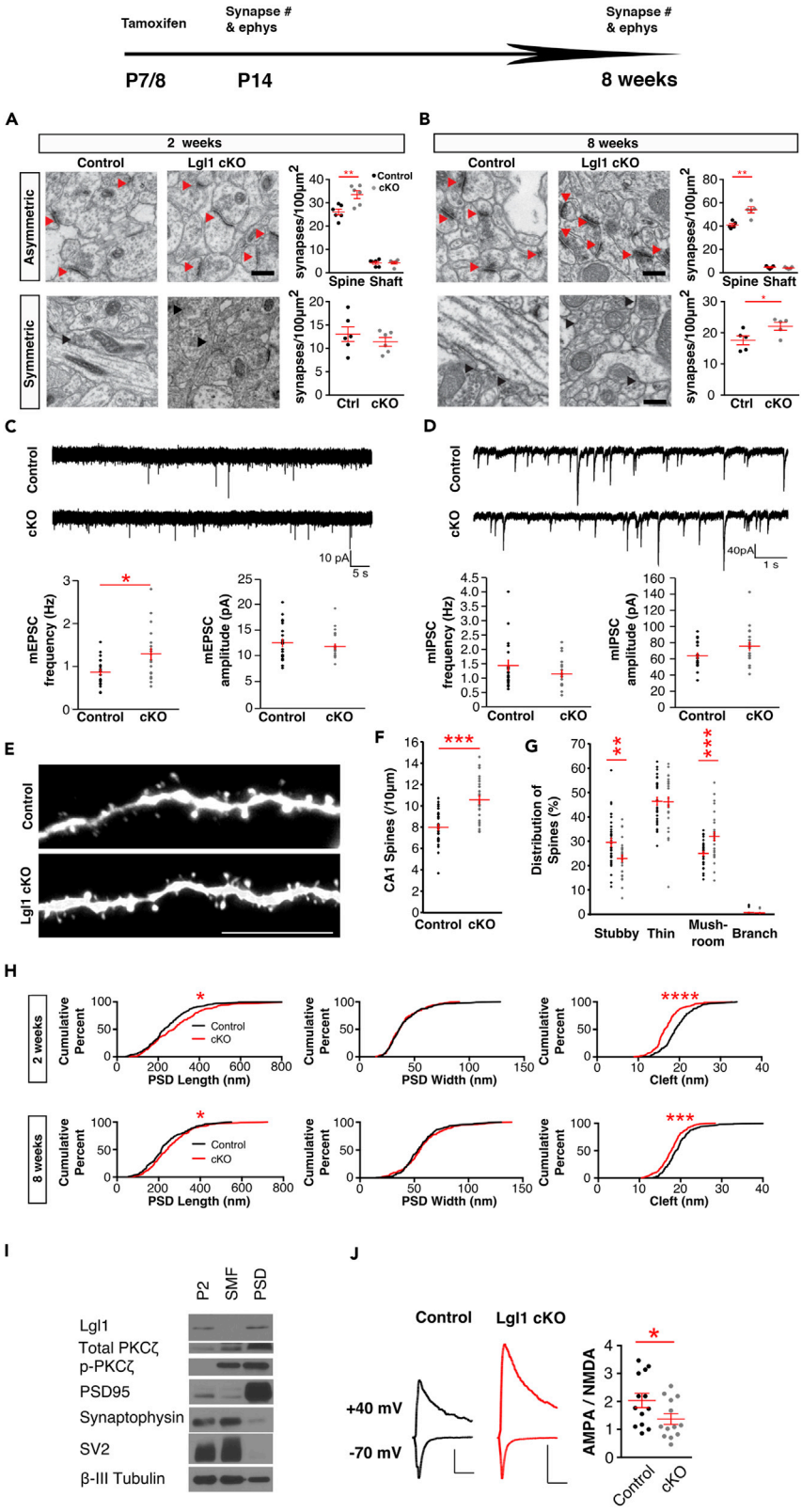
Tamoxifen
Synapse # & ephys
Synapse # & ephys
P7/8
P14
8 weeks
A
2 weeks
Control
Lgl1 cKO
Asymmetric
Symmetric
synapses/100μm2
Control
cKO
Spine Shaft
Ctrl cKO
B
8 weeks
C
D
10 pA
5 s
40pA
1 s
mEPSC frequency (Hz)
mEPSC amplitude (pA)
mIPSC frequency (Hz)
mIPSC amplitude (pA)
E
F
CA1 Spines (/10μm)
G
Distribution of Spines (%)
Stubby Thin Mush-room Branch
H
Cumulative Percent
PSD Length (nm)
PSD Width (nm)
Cleft (nm)
I
P2 SMF PSD
Lgl1
Total PKCζ
p-PKCζ
PSD95
Synaptophysin
SV2
β-III Tubulin
J
+40 mV
-70 mV
AMPA / NMDA

Figure 1. *Lgl1 Conditional Knockout* in Pyramidal Neurons Led to Increased Numbers of Asymmetric Synapses
(A) Electron micrographs taken 150–200 μm (top) or 50 μm (bottom) ventral to the CA1 pyramidal neuron layer in the schaffer collateral region of P14 mice. Red arrows denote asymmetric synapses. Black arrows denote symmetric synapses. Scale bar, 500 nm. Quantification of synapse numbers corresponding to each region: N = 6 control, 6 *Lgl1* cKO animals.
(B) Electron micrographs taken 150–200 μm (top) or 50 μm (bottom) ventral to the CA1 pyramidal neuron layer in the schaffer collateral region of 8-week-old mice. Red arrows denote asymmetric synapses. Black arrows denote symmetric synapses. Quantification of synapse numbers corresponding to each region: N = 5 control, 5 *Lgl1* cKO animals.
(C) Representative traces of mEPSC recordings from acute slices from P13–P15 control and *Lgl1* cKO mice. Quantification of mEPSC frequency and amplitude: n = 22 control, 19 *Lgl1* cKO neurons.
(D) Representative traces of mIPSC recordings from acute slices from P14 control and *Lgl1* cKO mice. Quantification of mIPSC frequency and amplitude: n = 20 control, 19 *Lgl1* cKO neurons.
(E) Representative confocal images of oblique CA1 dendrites filled with Alexa Fluor 555 hydrazide. Scale bar, 10 μm.
(F and G) (F) Quantification of spine density and (G) distribution of spine morphology.
(H) Quantification of cumulative distributions of synapse ultrastructure measurements in P14 control and cKO animals: n = 194 control, 174 *Lgl1* cKO synapses. Quantification of cumulative distributions of synapse ultrastructure measurements in 8-week old control and cKO animals: n = 194 control, 208 *Lgl1* cKO synapses.
(I) Biochemical fractionation from wild-type P14 mice. P2, crude synaptosomal; SMF, synaptic membrane fraction; PSD, postsynaptic density.
(J) Representative traces of NMDAR currents and combined AMPAR/NMDAR currents from acute slices taken from P14 control and *Lgl1* cKO mice following Lgl1 deletion at P7. Scale bar, 100 pA (vertical); 100 ms (horizontal). Quantification of the calculated ratio of AMPAR current to NMDAR current: n = 13 control, 13 *Lgl1* cKO neurons.
*$p < 0.05$; **$p < 0.01$; ***$p < 0.001$; ****$p < 0.0001$.

control and *Lgl1 cKO* animals. Quantification of frequency and amplitude of synaptic currents indicates that mEPSC frequency was increased by 38%, whereas amplitude was not changed significantly, indicating an increase in synapse number but similar AMPA-R composition (Figure 1C). No significant changes were observed in mIPSC currents (Figure 1D), consistent with our electron microscopy data. Consistent with this, cultured hippocampal neurons from mice carrying germline deletion of *Lgl1* also showed increased colocalization between PSD95 and vGlut1 puncta at 14 days *in vitro* (Figures S1F and S1G). mEPSC kinetics did not show significant changes (Figure S1H), whereas mIPSC kinetics only showed a significant decrease in decay time constant, but not in other measures (Figure S1I).

To determine whether dendritic spine density was affected, we filled neurons from fixed brain sections with Alexa 555 dye to visualize spines in yellow fluorescent protein (YFP)-positive CA1 pyramidal neurons (Figure 1E). We found that overall spine density was indeed increased by 38% in *Lgl1* cKO mice (Figure 1F). We also characterized the morphology of spines at P14. Compared with control, *Lgl1* cKO mice showed more mushroom spines and a reduced proportion of stubby spines (Figure 1G). As mushroom spines represent stabilized synapses and thin spines are unstable, this suggests that *Lgl1* cKO led to functionally hyperconnected circuits. Consistent with this, we then quantified the ultrastructure from the electron micrograph and found that the length of postsynaptic density (PSD) was increased and the gap of synaptic cleft was reduced at P14 and at age 8 weeks (Figure 1H). As Lgl1 interacts with the MAGUK proteins, we determined the subcellular localization and found that Lgl1 was present in the postsynaptic density (Figure 1I). We also measured AMPA/NMDA ratio, and found that the ratio is decreased in the *Lgl1 cKO*, suggesting altered glutamate receptor trafficking or function (Figure 1J).

Lgl1 Negatively Regulates Synapse Number by Inhibiting the Atypical PKCs

As Lgl1 and aPKC antagonize each other in cell polarity signaling, we asked whether Lgl1 may regulate synapse formation by inhibiting the aPKCs. To validate whether Lgl1 also inhibits the aPKCs in neurons, we tested their interaction in neural progenitor cells from E11.5 mouse telencephalon. *Lgl1* cKO and control cells were generated by treatment of cultures with AD5-CMV-Cre and Ad5-CMV-GFP adenoviruses (Vector Development Laboratory, Baylor College of Medicine), respectively, and verified that Lgl1 protein was completely lost in the cKO (Figure S2A). We then tested whether aPKC activity, as evident by association with Par3, was increased in *Lgl1* cKO. Activated aPKC (phosphorylated at T555) and aPKC interaction with Par3 were found strongly increased in *Lgl1* cKO, confirming the increase of apical signaling and decrease of basal-lateral signaling.

There are two isoforms of aPKCs in mouse. We used the same strategy of tamoxifen-induced deletion of *aPKCs* using *SLICK-H* to delete both isoforms of *aPKCs, PKCι/λ* and *PKCζ*, to eliminate the possibility of compensation. Following this deletion, we counted asymmetric and symmetric synapses from the schaffer

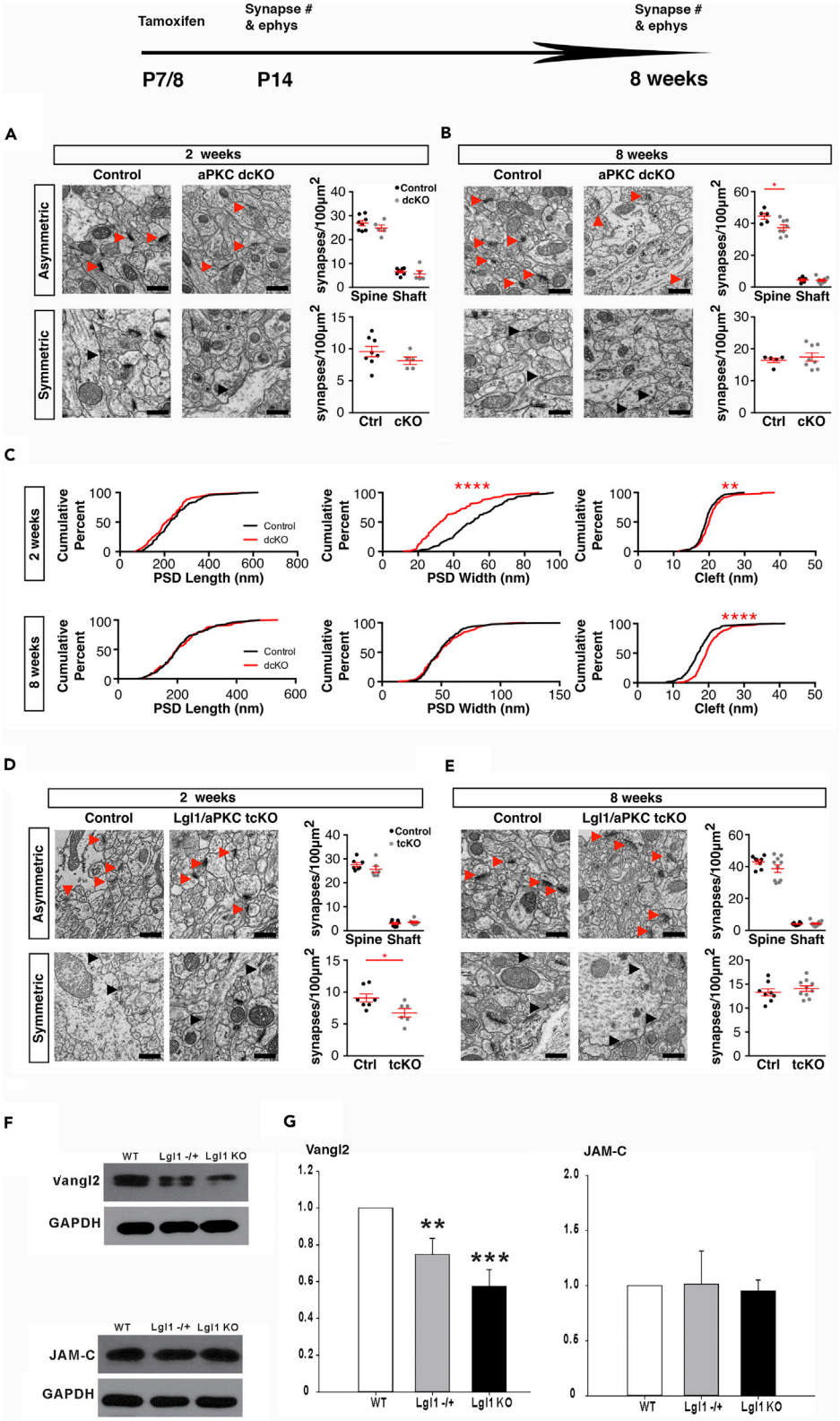
Tamoxifen
Synapse # & ephys
Synapse # & ephys
P7/8
P14
8 weeks
A
2 weeks
Control
aPKC dcKO
Asymmetric
Symmetric
synapses/100μm2
Control
dcKO
Spine Shaft
Ctrl cKO
B
8 weeks
C
2 weeks
8 weeks
Cumulative Percent
PSD Length (nm)
PSD Width (nm)
Cleft (nm)
D
Lgl1/aPKC tcKO
tcKO
E
F
WT Lgl1 -/+ Lgl1 KO
Vangl2
GAPDH
JAM-C
G

Figure 2. Lgl1 Inhibits Synapse Formation by Inhibiting aPKC and Promotes the Expression of Vangl2

(A) Electron micrographs taken 150–200 μm (top) or 50 μm (bottom) ventral to the CA1 pyramidal neuron layer in the schaffer collateral region of P14 mice. Red arrows denote asymmetric synapses. Black arrows denote symmetric synapses. Scale bar, 500 nm. Quantification of synapse numbers corresponding to each region: N = 8 control, 5 *aPKC dcKO* animals.

(B) Electron micrographs taken 150–200 μm (top) or 50 μm (bottom) ventral to the CA1 pyramidal neuron layer in the schaffer collateral region of 8-week-old mice. Red arrows denote asymmetric synapses. Black arrows denote symmetric synapses. Quantification of synapse numbers corresponding to each region: N = 5 control, 8 *aPKC dcKO* animals.

(C) Quantification of cumulative distribution of synapse ultrastructure measurements in P14 control and cKO animals: n = 194 control, 129 *aPKC dcKO* synapses. Quantification of cumulative distribution of synapse ultrastructure measurements in 8-week-old control and cKO animals: n = 87 control, 168 *aPKC dcKO* synapses.

(D) Electron micrographs taken 150–200 μm (top) or 50 μm (bottom) ventral to the CA1 pyramidal neuron layer in the schaffer collateral region of P14 mice. Red arrows denote asymmetric synapses. Black arrows denote symmetric synapses. Scale bar, 500 nm. Quantification of synapse numbers corresponding to each region: N = 7 control, 6 *Lgl1;PKCι/λ;PKCζ tcKO* animals.

(E) Electron micrographs taken 150–200 μm (top) or 50 μm (bottom) ventral to the CA1 pyramidal neuron layer in the schaffer collateral region of 8-week-old mice. Red arrows denote asymmetric synapses. Black arrows denote symmetric synapses. Quantification of synapse numbers corresponding to each region: N = 8 control, 10 *Lgl1;PKCι/λ;PKCζ tcKO* animals.

(F) Levels of Vangl2 and JAM-C proteins in P2 fractions by Western blots.

(G) Quantification of Vangl2 and JAM-C protein levels in P2 fraction. N = 5 for Vangl2. N = 4 for JAM-C.

*p < 0.05; **p < 0.01; ***p < 0.001; ****p < 0.0001.

collateral 150 μm from the CA1 cell layer of 2- and 8-week-old animals. At 2 weeks, we observed no significant difference in the number of asymmetric or symmetric synapses (Figure 2A). However, at 8 weeks, there was a significant decrease (−16.1%) in the number of asymmetric synapses (Figure 2B). In the proximal region 50 μm from the CA1 cell body layer, we also observed a significant decrease at 8 weeks, but not at 2 weeks (Figures S2B and S2C). Therefore, aPKC is not essential for initial glutamatergic synapse formation but required for their stability and maintenance. We then analyzed the ultrastructure and found that the PSD width was reduced at 2 weeks and the synaptic cleft was increased at 2 weeks and that the magnitude of this change increased at 8 weeks (Figure 2C). This suggests that aPKC is likely important for the stability of synapses, the opposite of Lgl1 (Figure 1H).

We then asked whether simultaneous deletion of *Lgl1*, *PKCι/λ*, and *PKCζ* might lead to mitigation of the effects observed in the *Lgl11* conditional deletion experiments. In 2-week-old *Lgl1:PKCι/λ:PKCζ* tcKO animals, we observe no significant change in asymmetric synapse number, suggesting that the increase of synapse numbers in *Lgl1 cKO* may be partly due to the increase of aPKC activity (Figure 2D). However, we observed a significant decrease (−25.9%) in the number of symmetric synapses. In 8-week-old *Lgl1:PKCι/λ:PKCζ* tcKO animals, we observed no significant change in asymmetric or symmetric synapse number (Figure 2E). No significant difference in asymmetric synapse density was observed in the proximal region at 2 and 8 weeks (Figures S3A and S3B). Therefore, Lgl1 may negatively regulate glutamatergic synapse numbers by inhibiting aPKC, which is required for the stability and maintenance of glutamatergic synapses.

Because PCP proteins regulate synapse formation and apical-basal polarity signaling regulates the localization PCP signaling components, we tested whether Lgl1 may regulate PCP components using synaptosome fractionation. The SLICK-H line (inducible Cre) expresses Cre in only 60% of pyramidal neurons at P7. Therefore, we cultured neurons from *Lgl1* KOs, heterozygotes, and wild-type and extracted synaptosome fraction. We found that Vangl2 protein levels are decreased in the P2 fractions of *Lgl1+/−* and *Lgl1−/−* compared with that of the *wild-type* (Figure 2F), whereas the levels of an adhesion molecule Jam-C were not affected (Figure 2G). This is consistent with the inhibitory function of Vangl2 in glutamatergic synapse formation.

Lgl1 Controls Glutamatergic Synapse Number and Is Required for Synaptic Plasticity in Adulthood

Because *Lgl1* is highly expressed in the adult central nervous system, including the hippocampus, we next characterized the role of Lgl1 in the adult brain. By early adulthood at age 6 weeks, synapse formation has slowed considerably in the rodent hippocampus compared with postnatal development (Wang et al., 2007). We conditionally knocked out *Lgl1* by injecting tamoxifen at 6 weeks after birth in SLICK-H animals.

We then used electron microscopy to assess the density of asymmetric and symmetric synapses in the schaffer collateral in 10-week-old animals. Asymmetric synapse density in the region 150–200 μm distal to the CA1 cell body layer was again increased by 28.6% on the dendritic spines (Figures 3A and 3B). A similar increase was observed in the proximal region 50 μm from the CA1 cell layer (Figures 3C and 3D). Symmetric synapses were again unaffected (Figures 3E and 3F). In addition, synapse ultrastructure was altered in the adult deletion of *Lgl1*, with longer and wider PSDs (Figures 3G and 3H) and smaller synaptic clefts (Figure 3I), possibly as a result of altered biochemical makeup of synapses. We performed patch clamping with P42 slices to assess the synaptic receptor expression from animals with *Lgl1* deleted beginning at P28. We observed a severe reduction in the AMPA/NMDA ratio in neurons from *Lgl1* cKO mice (Figures 3J and 3K), much greater than was observed at P14 following deletion of *Lgl1* at P7/P8. These results suggest that *Lgl1* is also required for control of synapse number and quality in adulthood.

We tested synaptic plasticity using hippocampal slices from 10-week old mice following conditional *Lgl1* deletion at age 6 weeks. Slices from *Lgl1* cKO animals showed impaired long-term potentiation induction in response to theta burst stimulation (TBS) (Figures 3L–3M). In addition, slices from *Lgl1* cKO mice showed impaired paired-pulse facilitation when stimuli were separated by 100 ms (Figure 3N), indicating altered synaptic release.

Lgl1 cKO Mice Showed Behavioral Deficits

Lgl1 is frequently deleted in SMS. But the genes responsible for the behavioral symptoms of SMS have not been well understood. To test whether deletion of *Lgl1* in pyramidal neurons may contribute to the behavioral deficits, we performed a number of behavioral tests. We assessed locomotor activity and exploratory behavior using an open field test (Figure 4A; Gould et al., 2009). *Lgl1 cKO* animals showed increased locomotor activity, traveling 20% further during the 10-min test than control mice (Figure 4B). No significant changes were observed in thigmotaxis, the preference for the outside of the field versus the center region (Figure 4C). Animals did not show a difference in the amount of time spent self-grooming during the open-field test (Figure S4A), but showed a significant increase in rearing activity, an exploratory behavior (Figure S4B).

To assess cognitive function following conditional *Lgl1* deletion, we tested the *Lgl1 cKO* crossed with SLICK-H in the novel object recognition (NOR) paradigm. The NOR test assesses whether an animal can distinguish a novel object from a previously explored familiar object. We calculated a preference index from each animal by subtracting the familiar object interaction time from the novel exploration time and normalizing to the total exploration time ((novel-familiar)/(novel + familiar)). During the sample phase, when both objects were novel, animals showed no preference and would randomly explore both objects (Figures 4D and 4E). When a novel object was introduced after a 2-min delay, control animals showed a strong preference for the novel object, whereas *Lgl1* cKO animals continued to explore randomly and maintain a preference index close to zero (Figures 4F and 4G).

Brain hyperconnectivity has been associated with ASDs (Dominguez et al., 2013; Keown et al., 2013; Supekar et al., 2013). Sociability in the three-chamber social interaction task has been used extensively to assess social behavior in mice (Yang et al., 2011). We tested *Lgl1 cKO* mice crossed with SLICK-H to assess their sociability (Figures 4H–4P). Before introduction of the target mouse, animals showed no preference for either side, exploring the field randomly (Figures 4H–4J). When a mouse was introduced to one side of the field, whereas an empty enclosure was introduced to the opposite side, control animals showed a strong preference for interacting with the novel mouse. *Lgl1 cKO* animals showed no preference (Figures 4K–4M) and spent similar amount of time exploring the novel mouse and novel object. Interestingly, no statistically significant difference was observed in the final phase of the test where subject mice were given a choice between a familiar and novel target mouse (Figures 4N–4P). Similar to controls, *Lgl1 cKO* mice still appeared to show a preference for the novel mouse. *Lgl1 cKO* mice showed normal spatial memory by alternations and entries in the Y-maze (Figures S4C and S4D) and normal visual performance (Figure S4E). Hippocampal- and amygdala-dependent memory formation was spared in the conditioned fear task (Figure S4F). Nestlet-shredding activity was unchanged in the conditional deletion of *Lgl1* (Figure S4G).

Atypical PKC Deletion Partially Rescued Behavioral Deficits of *Lgl1 cKO*

Having observed synapse phenotypes in the conditional *aPKC* deletion, we then tested whether the changes would lead to behavioral deficits. In open-field test, *PKCι/λ* and *PKCζ dcKO* animals showed no

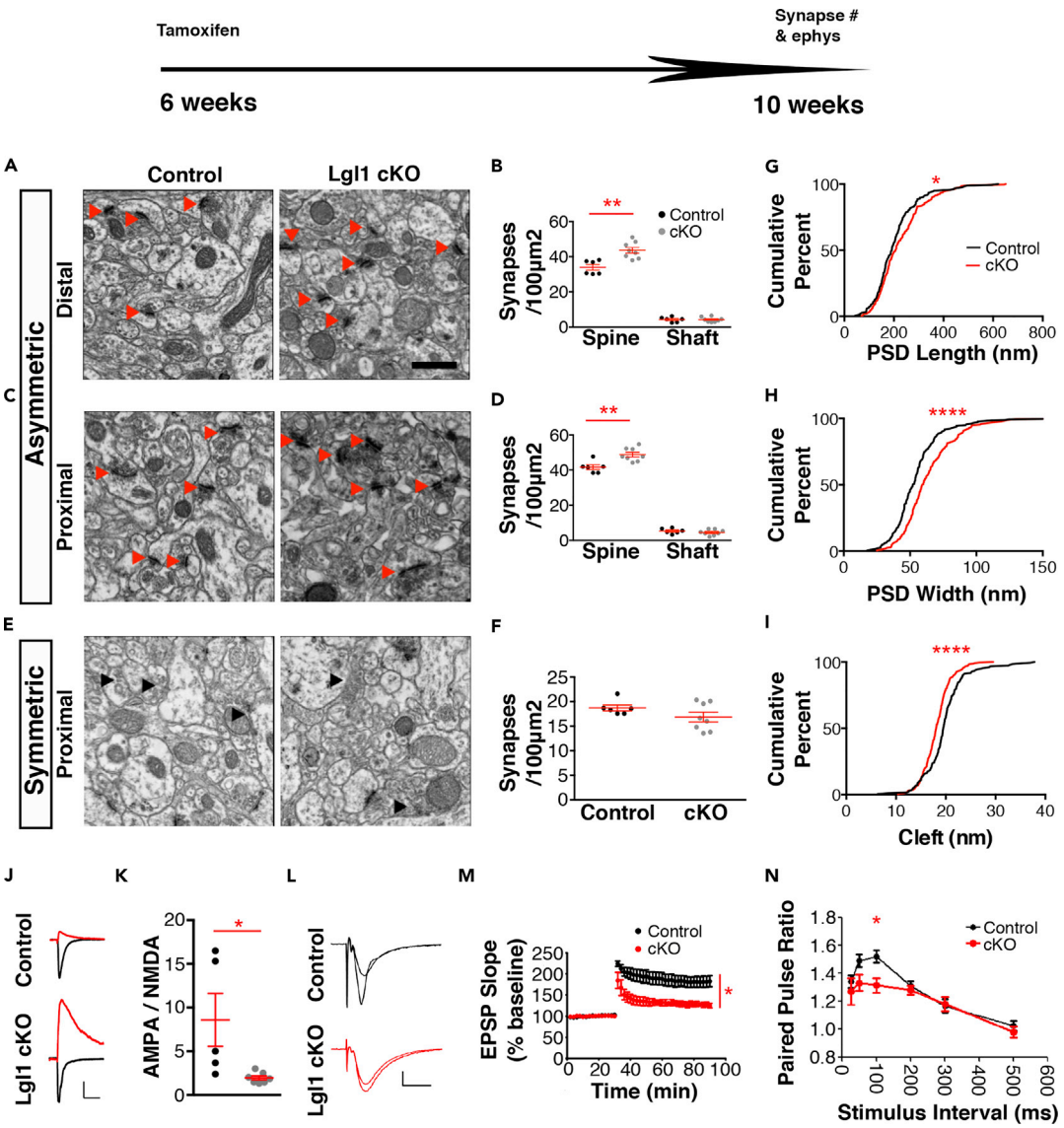

Figure 3. Increased Synapse Numbers, Altered AMPA/NMDA Ratio, and Impaired Plasticity in Adult Conditional Knockout of *Lgl1*

(A) Electron micrographs of the schaffer collateral (SC) 150–200 µm ventral to the CA1 pyramidal cell layer of slices from 10-week-old control and *Lgl1* cKO mice following deletion of Lgl1 beginning at 6 weeks of age. Red arrows denote asymmetric synapses. Scale bar, 500 nm. N = 6 control, 8 *Lgl1* cKO animals.

(B) Quantification of asymmetric synapse density of the region described in Figure 5A.

(C) Electron micrographs of the SC 50 µm ventral to the CA1 pyramidal cell layer in 10-week-old animals.

(D) Quantification of asymmetric synapses in the proximal region.

(E) Micrographs showing symmetric synapses (black arrows) in the proximal region of the SC.

(F) Quantification of symmetric synapses.

(G) Quantification of cumulative frequency for postsynaptic density (PSD) length.

(H) Quantification for PSD width.

(I) Quantification of synaptic cleft distance. n = 180 *Lgl1* control synapses, 242 *Lgl1* cKO synapses.

(J) Representative traces of NMDAR current and combined AMPAR/NMDAR current from acute slices taken from 6-week-old control and *Lgl1* cKO mice following Lgl1 deletion beginning at P28. Scale bar, 50 pA, 80 ms.

(K) Quantification of the calculated ratio of AMPAR to NMDAR current. N = 5 control, 7 *Lgl1* cKO neurons.

(L) Representative traces of EPSPs before and after TBS stimulation was delivered to acute slices from control and *Lgl1* cKO mice. Scale bar, 0.2 mV, 10 ms.

(M) Quantification of EPSP slope before and after theta burst stimulation (TBS). N = 5 *Lgl1* control, 4 *Lgl1* cKO.

(N) Quantification of paired-pulse ratio from control and *Lgl1* cKO animals deleted at 6 weeks. N = 6 *Lgl1* control, 6 *Lgl1* cKO.

*p < 0.05; **p < 0.01; ****p < 0.0001.

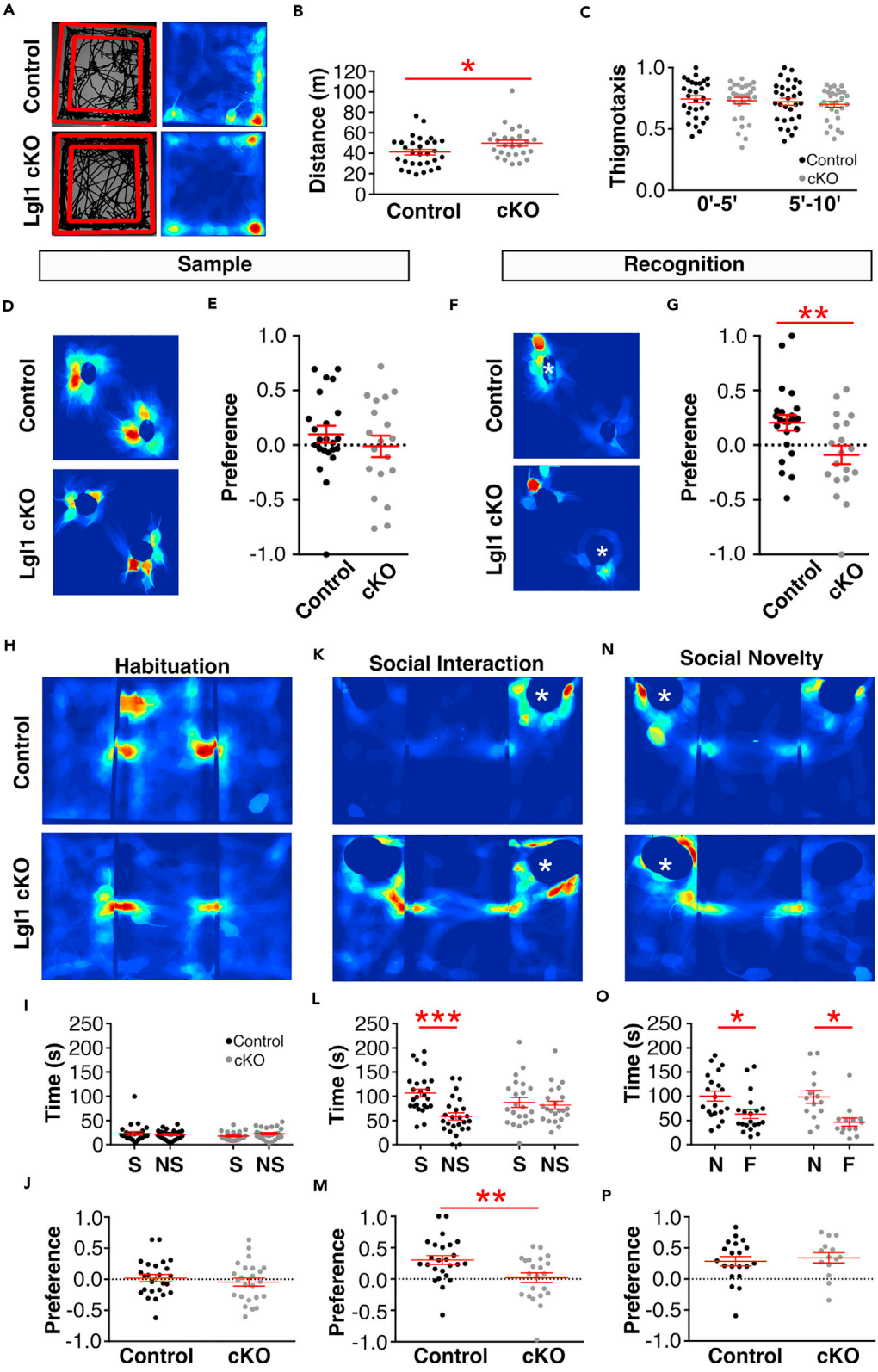
A
Control
Lgl1 cKO
B
Distance (m)
120
100
80
60
40
20
0
*
Control
cKO
C
Thigmotaxis
1.0
0.5
0.0
Control
cKO
0'-5'
5'-10'
Sample
Recognition
D
Control
Lgl1 cKO
E
Preference
1.0
0.5
0.0
-0.5
-1.0
Control
cKO
F
Control
Lgl1 cKO
*
*
G
**
Preference
1.0
0.5
0.0
-0.5
-1.0
Control
cKO
H
Habituation
Control
Lgl1 cKO
K
Social Interaction
*
*
N
Social Novelty
*
*
I
Time (s)
250
200
150
100
50
0
Control
cKO
S NS S NS
L
***
Time (s)
250
200
150
100
50
0
S NS S NS
O
*
*
Time (s)
250
200
150
100
50
0
N F N F
J
Preference
1.0
0.5
0.0
-0.5
-1.0
Control
cKO
M
**
Preference
1.0
0.5
0.0
-0.5
-1.0
Control
cKO
P
Preference
1.0
0.5
0.0
-0.5
-1.0
Control
cKO

Figure 4. *Lgl1* Deletion at P7 Produced a Subset of SMS-like Behavioral Phenotypes

(A) Open-field analysis following P7 deletion of Lgl1 showing representative trajectories (left) and heatmaps (right) of control and *Lgl1* cKO animals.

(B) Quantification of distance traveled during the test. N = 30 control, 27 *Lgl1* cKO.

(C) Quantification of time spent in the outer region of the field (thigmotaxis) during the first and second 5-min periods.

(D and E) (D) Representative heatmap and quantification (E) of animal preference for objects during the sample phase of the novel object recognition (NOR) test. N = 23 control, 19 *Lgl1* cKO animals.

(F and G) (F) Representative heatmaps and quantification (G) of animal preference for objects during the test phase of the NOR test. White asterisk denotes location of the novel object.

(H) Representative heatmaps from the habituation period of the social interaction (SI) test.

(I and J) (I) Quantification of time spent in and (J) preference for regions of interest (ROIs) representing future location of novel mice and objects. N = 25 control, 24 *Lgl1* cKO animals.

(K) Representative heatmaps during the social interaction phase of the SI test. White asterisk denotes location of the novel mouse. Opposite chamber contains the object.

(L and M) (L) Quantification of time spent in and (M) preference for ROIs containing either the novel mouse or novel object. Positive value indicates preference for the novel mouse. N = 25 control, 22 *Lgl1* cKO animals.

(N) Representative heatmaps during the social novelty phase of the SI test. White asterisk denotes location of the novel mouse. Opposite chamber contains the previously explored mouse.

(O and P) (O) Quantification of time spent interacting with and (P) preference for mice during the social novelty phase. Positive value indicates preference for the novel mouse. N = 20 control, 14 *Lgl1* cKO animals. NS, nonsocial; S, social. *p < 0.05; **p < 0.01; ***p < 0.001.

significant changes in locomotor activity or thigmotaxis (Figures 5A–5C). We also assessed cognitive function and found that *PKCι/λ:PKCζ dcKO* were impaired in the novel object recognition test (Figures 5D and 5E). In the social interaction test, animals showed no preference before the introduction of the novel mouse (Figures 5F and 5G). Littermate control animals preferred social interaction, spending more time with the novel mouse versus the novel object, whereas *PKCι/λ:PKCζ dcKO* spent similar amounts of time interacting with the novel mouse and novel object, maintaining a preference index close to 0 (Figures 5H and 5I). Preference for social novelty was unaffected by aPKC deletion (Figures 5J and 5K).

We then tested locomotor activity and observed no difference between littermate control and *Lgl1:PKCι/λ:PKCζ* tcKO animals (Figures 5L–5M). However, triple conditional deletion of *Lgl1*, *PKCι/λ*, and *PKCζ* did rescue cognitive deficit in the novel object recognition test, with *Lgl1:PKCι/λ:PKCζ* tcKO animals performing similarly to littermate controls and better than chance (one-sample t test, p = 0.0262) in the test (Figures 5N–5Q). Our observations showed that conditional deletion of *Lgl1*, *PKCι/λ*, and *PKCζ* corrects synapse density changes observed and preserves cognitive function. In the social interaction test (Figures 5R–5W), tcKO animals still showed impairment in the social interaction phase (Figures 5T–5U), but not the social novelty phase (Figures 5V–5W).

Lgl1 Heterozygotes Had Increased Synapse Numbers and Displayed Behavioral Deficits Suggesting a Role in Smith-Magenis Syndrome

As SMS arises from heterozygous deletion of the critical region, we assessed the effects of germline heterozygous deletion of *Lgl1* in our mouse (Klezovitch et al., 2004). We imaged hippocampal sections from 8-week-old control and *Lgl1* heterozygous animals from the germline *Lgl1* KO line using electron microscopy. In these animals, the region 150–200 μm from the CA1 cell body layer showed an increase in asymmetric synapse density, with a somewhat smaller but significant increase (22.6%; Figure 6A and proximal region: S5A) compared with what was observed when both copies were deleted in the conditional KO. Symmetric synapses were not affected. Analysis of synapse ultrastructure revealed longer and wider PSDs and smaller synaptic clefts (Figure 6B).

In the open-field test, *Lgl1*+/− animals did not show a significant difference from control animals after 10 min (Figures S5B and S5C). During an extended observation period of 60 min in the open field (Figure 6C), $Lgl1^{+/-}$ animals showed increased locomotor activity by 12.0% overall.

We also tested stereotyped repetitive behavior and found that *Lgl1*+/− animals showed increased nestlet shredding when given cotton nesting material in a novel cage (Figure 6D), shredding 59.4% more material during the test. As this behavior was not observed in *Lgl1* cKO, this is likely a result of *Lgl1* deletion in heterozygotes in the subcortical areas that are not affected by the *Thy-1*-dependent deletion in the *Lgl1* cKO animals crossed with SLICK-H.

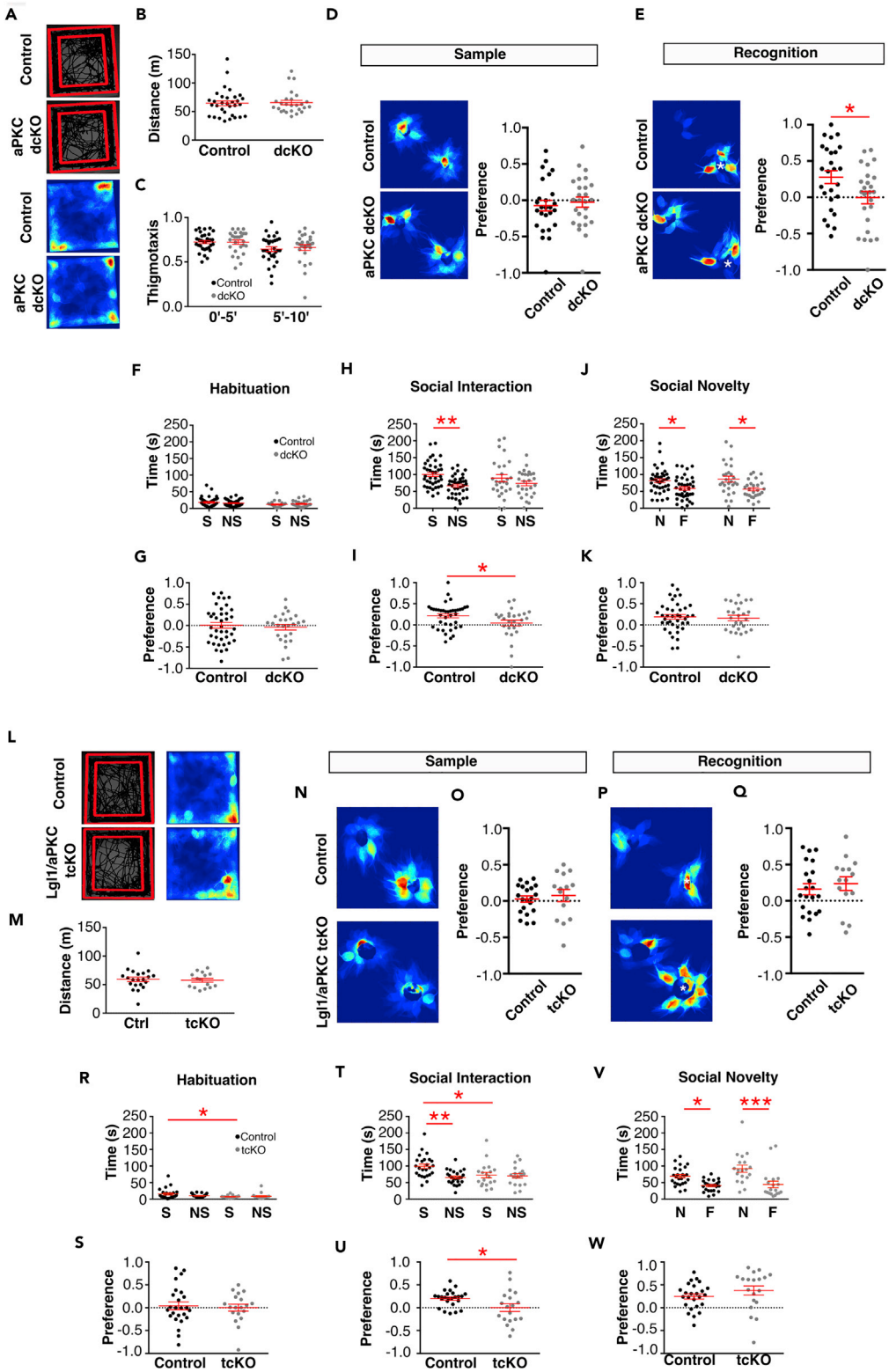

Figure 5. Conditional Triple Knockout of Lgl1, PKCι/λ, and PKCζ Rescued Asymmetric Synapse Number and Cognitive Deficit

(A) Open-field analysis following P7 deletion of Lgl1 showing representative trajectories (left) and heatmaps (right) of control and *aPKC dcKO* animals.

Figure 5. *Continued*

(B) Quantification of distance traveled during the test. N = 32 control, 26 *aPKC dcKO* animals.

(C) Quantification of time spent in the outer region of the field (thigmotaxis) during the first and second 5-min periods.

(D) Representative heatmap and quantification of animal preference for objects during the sample phase of the novel object recognition (NOR) test. N = 26 control, 15 *aPKC dcKO* animals.

(E) Representative heatmaps and quantification of animal preference for objects during the test phase of the NOR test. White asterisk denotes location of the novel object.

(F and G) (F) Quantification of time spent in and (G) preference for regions of interest (ROIs) representing future location of novel mice and objects. N = 35 control, 26 *aPKC dcKO* animals.

(H and I) (H) Quantification of time spent in and (I) preference for ROIs containing either the novel mouse or novel object. Positive value indicates preference for the novel mouse. N = 35 control, 27 *aPKC dcKO* animals. *p < 0.05; **p < 0.01.

(J and K) (J) Quantification of time spent interacting with and (K) preference for target mice during the social novelty phase. Positive value indicates preference for the novel mouse. N = 35 control, 27 *aPKC dcKO* animals. *p < 0.05.

(L) Open-field analysis following P7 deletion showing representative trajectories (left) and heatmaps (right) of control and *Lgl1;PKCι/λ;PKCζ tcKO* animals.

(M) Quantification of distance traveled during the test. N = 20 control, 14 *Lgl1;PKCι/λ;PKCζ tcKO* animals.

(N and O) (N) Representative heatmap and quantification (O) of animal preference for objects during the sample phase of the novel object recognition (NOR) test. N = 21 control, 15 *Lgl1;PKCι/λ;PKCζ tcKO* animals.

(P and Q) (P) Representative heatmaps and quantification (Q) of animal preference for objects during the recognition test phase of the NOR test. White asterisk denotes location of the novel object.

(R and S) (R) Quantification of time spent in and (S) preference for ROIs representing future location of novel mice and objects.

(T and U) (T) Quantification of time spent in and (U) preference for ROIs containing either the novel mouse or novel object. Positive value indicates preference for the novel mouse.

(V and W) (V) Quantification of time spent interacting with and (W) preference for target mice during the social novelty phase. Positive value indicates preference for the novel mouse. N = 25 control, 19 *Lgl1;PKCι/λ;PKCζ tcKO* animals. NS, nonsocial; S, social.

*p < 0.05; **p < 0.01; ***p < 0.001.

Preference for novel object recognition was spared in *Lgl*+/− animals (Figures S5E–S5H) following a 2-min delay, suggesting that this cognitive task might be partially spared by either reduced impact on synapse density or synaptic function due to the remaining copy of *Lgl1*. Therefore, we performed an additional novel object recognition test, this time with a 24-h delay between the initial sample period and the recognition test. After 24 h, control animals successfully discriminated novel and familiar objects, whereas *Lgl1*+/− animals did not (Figure 6E). Patients with SMS demonstrate mild to moderate cognitive impairment or developmental delay, and it is likely that the partially preserved recognition of novel objects reflects a mild cognitive impairment in the mouse model.

Similar to *Lgl1* cKO animals, *Lgl1*+/− animals demonstrated deficient social interaction, but spared preference for social novelty (Figures 6F, S5I, and S5J), indicating that loss of one copy of *Lgl1*—as occurs in SMS—may be sufficient to give rise to ASD-like behaviors. *Lgl1*+/− animals did not show a difference from control littermates in age-dependent weight gain (Figure S5K).

Social Interaction Deficit in *Lgl1+/−* May Be Caused by Excessive NMDA Current

Because SMS often presents with either seizures or abnormal EEG without overt seizure (Chen et al., 1996; Greenberg et al., 1996), we tested whether abnormally high synapse density and NMDA current would lower the seizure threshold in response to the $GABA_A$-blocking drug pentylenetetrazol (PTZ). Following injection of 50 mg/kg PTZ, the occurrence and latency of activities indicating the onset of a seizure were recorded. All animals tested showed at least one instance of jumping or full-body jerking (Figure 7A), whereas *Lgl1+/−* animals showed a shorter latency to the behavior following PTZ administration (Figure 7B). *Lgl1+/−* animals also showed significantly higher occurrence and shorter latency to Straub Tail, indicating persistent muscle contraction, and also showed a similar effect for the occurrence of clonic-tonic seizures.

The lower AMPA/NMDA ratio and unaffected AMPA current suggests that *Lgl1* mutants may have excessive NMDA current. We asked whether abnormal NMDAR-dependent signaling could underlie some of the behavioral deficit, especially social interaction, that we observed. We used pharmacological blockers of NMDARs and tested animals in the three-chamber social interaction test. Subanesthetic dose of ketamine has been shown to provide rapid blockage of NMDAR-dependent signaling. We tested social interaction with injection of 50 μL sterile saline and observed that control animals preferred social interaction, whereas *Lgl1+/−* mice did not show a preference (Figures 7C–7E). Following injection of 30 mg/kg

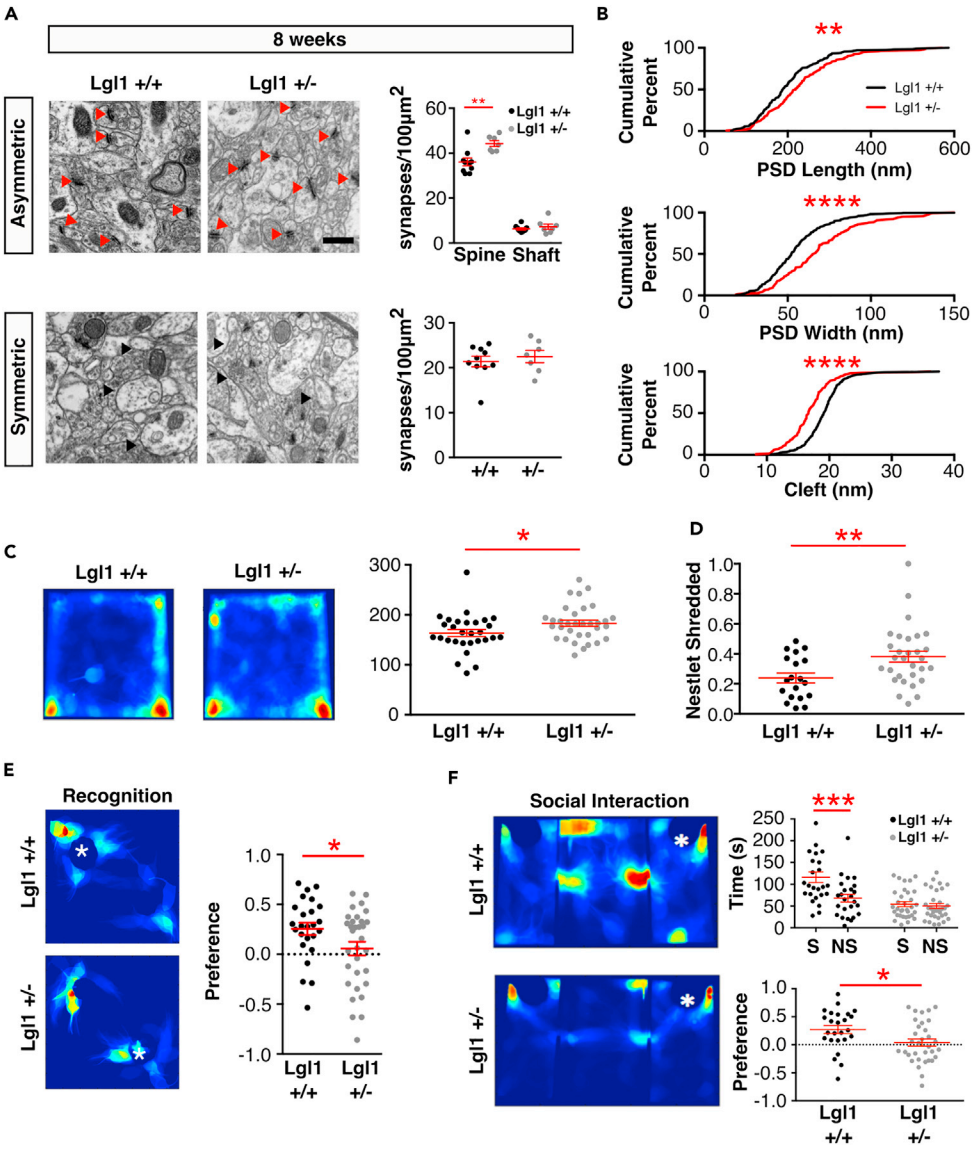

Figure 6. *Lgl1*+/− Mice Showed Increased Synaptic Numbers and SMS-like Behavioral Phenotypes

(A) Electron micrographs taken 150–200 μm (top) or 50 μm (bottom) ventral to the CA1 pyramidal neuron layer in the schaffer collateral region of 8-week-old mice. Red arrows denote asymmetric synapses. Black arrows denote symmetric synapses. Scale bar, 500 nm. Quantification of synapse numbers corresponding to each region: N = 10 *Lgl1*+/−, 7 *Lgl1*+/− animals.

(B) Quantification of cumulative distribution of synapse ultrastructure measurements in 8-week old *Lgl1*+/+ and *Lgl1*+/− animals: n = 265 *Lgl1*+/+ synapses, 140 *Lgl1*+/− synapses.

(C) Representative heatmaps from the 1-h extended-duration open-field test for *Lgl1*+/+ and *Lgl1*+/− animals and quantification for distance traveled in the extended open-field test. N = 30 *Lgl1*+/+, 33 *Lgl1*+/−.

(D) Quantification of nestlet-shredding activity. N = 19 *Lgl1*+/+, 30 *Lgl1*+/− animals.

(E and F) (E) Representative heatmaps from the recognition test phase of the novel object recognition (NOR) test 24 h after the sample phase of the object. Quantification of object preference during the test phase 24 h after the sample phase. N = 25 *Lgl1*+/+, 32 *Lgl1*+/−. (F) Representative heatmaps during the social interaction phase of the social interaction (SI) test. White asterisk denotes location of the novel mouse. Quantification of interaction preference in the SI test. N = 25 *Lgl1*+/+, 33 *Lgl1*+/− animals.

*p < 0.05; **p < 0.01; ***p < 0.001; ****p < 0.0001.

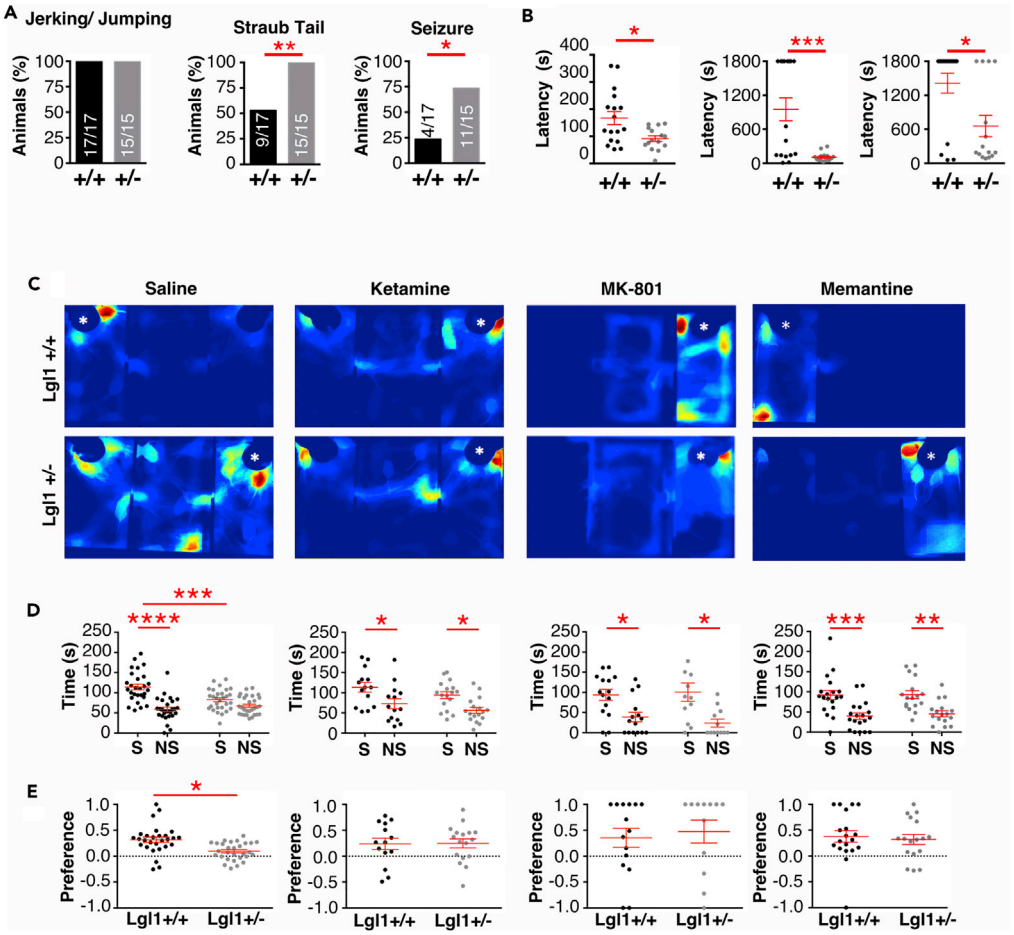

Figure 7. Decreased Seizure Threshold in *Lgl1*+/− Mice and Rescue of Social Interaction by NMDAR Blockade

(A) Quantification of the occurrence of jerking/jumping, Straub tail, and clonic-tonic seizures in *Lgl1*+/+ and *Lgl1*+/− animals following 50 mg/kg PTZ administration. Fisher's exact test.

(B) Quantification of the latency to the first observation of behaviors following 50 mg/kg PTZ administration. N = 17 *Lgl1*+/+, 15 *Lgl1*+/− animals. Mann-Whitney U statistic test.

(C) Representative heatmaps during the social interaction phase of the social interaction test following intraperitoneal injection with 50 μL saline, 30 mg/kg ketamine, 0.3 mg/kg MK-801, or 20 mg/kg memantine. White asterisk denotes location of the novel mouse.

(D and E) (D) Quantification of time spent in social (S) or nonsocial (NS) regions of interest and (E) interaction preference of treated animals. N = (saline) 17 *Lgl1*+/+, 19 *Lgl1*+/− animals; (ketamine) 14 *Lgl1*+/+, 17 *Lgl1*+/− animals; (MK-801) 13 *Lgl1*+/+, 14 *Lgl1*+/− animals; (memantine) 19 *Lgl1*+/+, 17 *Lgl1*+/− animals.

*p < 0.05; **p < 0.01; ***p < 0.001; ****p < 0.0001.

ketamine, *Lgl1*+/− mice showed a clear preference for social interaction similar to what was observed from control animals (Figures 7C–7E). Preferences in habituation and social novelty phases are unaffected by saline or drug injection (Figures S6A–S6D). Ketamine injection did not change nestlet-shredding activity (Figure S6E). In addition, we also tested MK-801 (dizocilpine) at 0.3 mg/kg and memantine at 20 mg/kg and observed that *Lgl1*+/− strongly preferred social interaction, as did control mice (Figures 7C–7E). These results suggest that excessive NMDA current due to *Lgl1* deletion may contribute to some of the behavioral deficits and that inhibiting NMDARs may help alleviate some of the neuropsychiatric symptoms in SMS patients with *Lgl1* deletion.

DISCUSSION

Although many of the proteins in glutamatergic synapses have been identified and their roles in synapse formation and function have been studied, the signaling logic that orchestrates the assembly of hundreds

of proteins into a highly organized and dynamic structure remains poorly known. We show here that a conserved apical-basal polarity signaling component, Lgl1, is localized in the PSD and regulates synapse numbers and compositions of key synaptic proteins and glutamate receptors, probably by inhibiting aPKC activity and via interactions with its conserved binding partners, particularly the MAGUKs. Atypical PKC has been studied for its role in memory formation and consolidation. Here we report that conditional deletion of both isoforms of aPKCs at P7 and P8 led to a reduction in synapse number in adulthood and cognitive and social deficits. The observation that deletion of Lgl1 or aPKC both lead to behavioral changes indicates that synapse number must be optimally controlled for behavioral functions and changes in either direction lead to impairment. Triple conditional knockout of Lgl1 and aPKC isoforms rescued the number of the asymmetric synapses and cognitive function, supporting their antagonistic functions in synapse formation. Lgl1 forms a basal complex with Discs Large, which is the homolog of MAGUKs, essential scaffold proteins in the postsynaptic density, which regulate trafficking and clustering of glutamate receptors. Therefore, loss of Lgl1 may lead to changes of MAGUKs and glutamate receptor compositions, such as the reduction of AMPA/NMDA ratio. It should be noted that we also observed a decrease of paired-pulse ratio in *Lgl1 cKO*, suggesting that there may also be presynaptic defects (Figure 3N). The Cre line we used here, *SLICK-H*, expresses CreERT2 in both CA3 and CA1 pyramidal neurons. Although Lgl1 was found to be present in the postsynaptic density (Figure 1I), Lgl1 may also have a function on the presynaptic side. This reduction of paired-pulse ratio may contribute to the altered synaptic function.

Lgl1 is frequently deleted in SMS; therefore, we performed a number of behavioral tests. cKO of *Lg11* from P7 and P8 led to behavioral deficits, including hyperactivity, cognitive impairment, and social interaction, consistent with the autism-like symptoms in SMS. As SMS involves the microdeletion of one of the chromosomes, we analyzed the *Lgl1+/−* mice and found that *Lgl1+/−* mice had increased synapse numbers, impaired social interaction, and increased stereotyped repetitive behavior, suggesting that *Lgl1* is a candidate gene that contributes to the autism-like symptoms of SMS with *Lgl1* deletion. Repetitive behaviors involve the striatum, where $CreER^{T2}$ is not expressed in the SLICK-H line. This may explain why repetitive behavior defects were only observed in *Lgl1+/−*. There was a slowed habituation to the open field in *Lgl1+/−* and defects in novel object recognition. In summary, loss of both copies of *Lgl1* locally or only one copy of *Lgl1* globally could cause behavioral deficits related to a subset of autism-like symptoms of SMS. Interestingly, *Lgl1* cKO and *Lgl1+/−* animals did not show an increase in grooming behavior during open-field observation or signs of excessive self-grooming while in their home cage that characterizes other ASD-like mouse models (Peça et al., 2011). Lgl1 appears to be important to maintaining proper synapse numbers and normal function of synapses even in adulthood as deleting *Lgl1* at 6 weeks still lead to increase of synapse numbers and changes of synapse structure and function. *Lgl1* may be a key molecule required for synaptic plasticity in adulthood as cKO led to impairment of long-term potentiation. Therefore the loss of *Lgl1* in SMS may underlie the neurobiological basis of behavioral symptoms. We propose that *Lgl1* is a candidate gene contributing to SMS. Our studies also give rise to a mouse model (*Lgl1+/−* mice) for SMS for understanding disease mechanisms and development of treatment. Indeed, we found that blockade of NMDARs rescues social deficits, suggesting that NMDARs may be promising therapeutic targets for SMS with *Lgl1* deletion.

Limitations of the Study

In Figure 3K, the variability of the data is greater for the control compared to the *Lgl1* cKO. This is a weakness of our data. However, upon closer inspection of the results, all but one of the data points in the control are higher than all data points from the conditional knockout. Therefore, while the data quality is not ideal, we believe that the conclusion would hold even with a larger sample size.

METHODS

All methods can be found in the accompanying Transparent Methods supplemental file.

SUPPLEMENTAL INFORMATION

Supplemental Information can be found online at https://doi.org/10.1016/j.isci.2019.09.005.

ACKNOWLEDGMENTS

This work was supported by NIMH RO1 MH116667, NIMH R21 MH099082, and a March of Dimes grant to Y.Z., NIH Training grant Fellowships to S.T. (T32 NS007220-27) and J.S. (T32 GM007240-36), and 2014

NARSAD Young Investigator Award to S.T. We thank the Electron Microscopy Core Facility at UCSD School of Medicine for sample preparation and technical assistance and the Mouse Behavioral Assessment Core at the Scripps Research Institute for behavioral tests and helpful suggestions.

AUTHOR CONTRIBUTIONS

Y.Z. and J.S. designed the experiments. J.S., S.T., Y.M., H.Q., H.H., S.-Y.L., and T.Y. performed the experiments and analyzed the results. O.K. and V.V. provided the Lgl1 KO and cKO mice. H.C., Y.M., and S.G. provided aPKC cKOs. Y.Z. and J.S. wrote the manuscript.

DECLARATION OF INTERESTS

Y.Z. is the founder of VersaPeutics and VersaChem. The terms of this arrangement have been reviewed and approved by the University of California, San Diego, in accordance with its conflict of interest policies.

Received: June 18, 2019
Revised: August 25, 2019
Accepted: September 4, 2019
Published: October 25, 2019

REFERENCES

Betschinger, J., Mechtler, K., and Knoblich, J.A. (2003). The Par complex directs asymmetric cell division by phosphorylating the cytoskeletal protein Lgl. Nature *422*, 326–330.

Chen, K., Manian, P., Koeuth, T., Potocki, L., Zhao, Q., Chinault, A., Lee, C., and Lupski, J. (1997). Homologous recombination of a flanking repeat gene cluster is a mechanism for a common contiguous gene deletion syndrome. Nat. Genet. *17*, 154–163.

Chen, K.-S., Potocki, L., and Lupski, J.R. (1996). The smith-magenis syndrome [del(17)p11.2]: clinical review and molecular advances. Ment. Retard. Dev. Disabil. Res. Rev. *2*, 122–129.

Chuykin, I., Ossipova, O., and Sokol, S.Y. (2018). Par3 interacts with Prickle3 to generate apical PCP complexes in the vertebrate neural plate. Elife *7*, https://doi.org/10.7554/eLife.37881.

Collingridge, G., Kehl, S., and McLennan, H. (1983). Excitatory amino acids in synaptic transmission in the Schaffer collateral-commissural pathway of the rat hippocampus. J. Physiol. *334*, 33–46.

Dominguez, L., Stieben, J., Velazquez, J., and Shanker, S. (2013). The imaginary part of coherency in autism: differences in cortical functional connectivity in preschool children. PLoS One *8*, 1–13.

Dykens, E., Finucane, B., and Gayley, C. (1997). Brief report: cognitive and behavioral profiles in persons with smith-magenis syndrome. J. Autism. Dev. Disord. *27*, 203–211.

Dykens, E., and Smith, A.C.M. (1998). Distinctiveness and correlates of maladaptive behaviour in children and adolescents with Smith-Magenis syndrome. J. Intellect. Disabil. Res. *42*, 481–489.

Edelman, E., Girirajan, S., Finucane, B., Patel, P., Lupski, J., Smith, A., and Elsea, S. (2007). Gender, genotype, and phenotype differences in Smith–Magenis syndrome: a meta-analysis of 105 cases. Clin. Genet. *71*, 540–550.

Georgiou, M., Marinari, E., Burden, J., and Baum, B. (2008). Cdc42, Par6, and aPKC regulate Arp2/3-mediated endocytosis to control local adherens junction stability. Curr. Biol. *18*, 1631–1638.

Girirajan, S., Vlangos, C., Szomju, B., Edelman, E., Trevors, C., Dupuis, L., Nezarati, M., Bunyan, D., and Elsea, S. (2006). Genotype-phenotype correlation in Smith-Magenis syndrome: Evidence that multiple genes in 17p11.2 contribute to the clinical spectrum. Genet. Med. *8*, 417–427.

Gould, T., Dao, D., and Kovacsics, C. (2009). The open field test. In Mood and Anxiety Related Phenotypes in Mice, *42* (Humana Press), pp. 1–20.

Greenberg, F., Lewis, R.A., Potocki, L., Glaze, D., Parke, J., Killian, J., Murphy, M.A., Williamson, D., Brown, F., Dutton, R., et al. (1996). Multi-disciplinary clinical study of smith-magenis syndrome (deletion 17p11.2). Am. J. Med. Genet. *62*, 247–254.

Gropman, A., Elsea, S., Duncan, W., and Smith, A. (2007). New developments in Smith-Magenis syndrome (del 17p11.2). Curr. Opin. Neurol. *20*, 125–134.

Heimer-McGinn, V., and Young, P. (2011). Efficient inducible Pan-neuronal cre-mediated recombination in SLICK-H transgenic mice. Genesis *49*, 942–949.

Huang, W.H., Guenther, C.J., Xu, J., Nguyen, T., Schwarz, L.A., Wilkinson, A.W., Gozani, O., Chang, H.Y., Shamloo, M., and Luo, L. (2016). Molecular and neural functions of rai1, the causal gene for smith-magenis syndrome. Neuron *92*, 1–15.

Karner, C., Wharton, K.A., and Carroll, T.J. (2006). Apical-basal polarity, Wnt signaling and vertebrate organogenesis. Semin. Cell Dev. Biol. *17*, 214–222.

Keown, C., Shih, P., Nair, A., Peterson, N., Mulvey, M., and Muller, R. (2013). Local functional overconnectivity in posterior brain regions is associated with symptom severity in autism spectrum disorders. Cell Rep. *5*, 567–572.

Klezovitch, O., Fernandez, T.E., Tapscott, S.J., and Vasioukhin, V. (2004). Loss of cell polarity causes severe brain dysplasia in Lgl1 knockout mice. Genes Dev. *18*, 559–571.

Koyama, K., Fukushima, Y., Inazawa, J., Tomotsune, D., Takahashi, N., and Nakamura, Y. (1996). The human homologue of the murine Llglh gene (LLGL) maps within the Smith-Magenis syndrome region in 17p11.2. Cytogenet. Cell Res. *72*, 78–82.

Laje, G., Morse, R., Richter, W., Ball, J., Pao, M., and Smith, A. (2010). Autism spectrum features in Smith-Magenis syndrome. Am. J. Med. Genet. C Semin. Med. Genet. *154*, 456–462.

Macara, I.G. (2004). Parsing the polarity code. Nat. Rev. Mol. Cell Biol. *5*, 220–231.

Martin, S., Wolters, P., and Smith, A. (2006). Adaptive and maladaptive behavior in children with smith-magenis syndrome. J. Autism. Dev. Disord. *36*, 541–552.

Monaghan, D.T., Bridges, R.J., and Cotman, C.W. (1989). The excitatory amino acid receptors: their classes, pharmacology, and distinct properties in the function of the central nervous system. Annu. Rev. Pharmacol. Toxicol. *29*, 365–402.

Peça, J., Feliciano, C., Ting, J., Wang, W., Wells, M., Venkatraman, T., Lascola, C., Fu, Z., and Feng, G. (2011). Shank3 mutant mice display autistic like behaviours and striatal dysfunction. Nature *472*, 437–442.

Potocki, L., Shaw, C., Stankiewicz, P., and Lupski, J. (2003). Variability in clinical phenotype despite commonchromosomal deletion in Smith-Magenis syndrome[del(17)(p11.2p11.2)]. Genet. Med. *5*, 430–434.

Smith, A.C., Dykens, E., and Greenberg, F. (1998). Behavioral phenotype of Smith-Magenis syndrome (del 17p11.2). Am. J. Med. Genet. *81*, 179–185.

Smith, A.C.M., McGavran, L., Robinson, J., Waldstein, G., Macfarlane, J., Zonona, J., Reiss, J., Lahr, M., Allen, L., and Magenis, E. (1986). Interstitial deletion of (17)(p11.2p11.2) in nine patients. Am. J. Med. Genet. A *24*, 393–414.

Supekar, K., Uddin, L., Khouzam, A., Phillips, J., Gaillard, W., Kenworthy, L., Yerys, B., Vaidya, C., and Menon, V. (2013). Brain hyperconnectivity in children with autism and its links to social deficits. Cell Rep. *5*, 738–747.

Thakar, S., Wang, L., Yu, T., Ye, M., Onishi, K., Scott, J., Qi, J., Fernandes, C., Han, X., Yates, J.R., 3rd, et al. (2017). Evidence for opposing roles of Celsr3 and Vangl2 in glutamatergic synapse formation. Proc. Natl. Acad. Sci. U S A *114*, E610–E618.

Vlangos, C.N., Yim, D.K.C., and Elsea, S.H. (2003). Refinement of the Smith–Magenis syndrome critical region to 950 kb and assessment of 17p11.2 deletions. Are all deletions created equally? Mol. Genet. Metab. *79*, 134–141.

Wang, R., Tang, Y., Feng, B., Ye, C., Fang, L., Zhang, L., and Li, L. (2007). Changes in hippocampal synapses and learning-memory abilities in age-increasing rats and effects of tetrahydroxystilbene glucoside in aged rats. Neuroscience *149*, 739–746.

Watkins, J.C., and Evans, R.H. (1981). Excitatory amino acid transmitters. Annu. Rev. Pharmacol. Toxicol. *21*, 165–204.

Yamanaka, T., Horikoshi, Y., Izumi, N., Suzuki, A., Mizuno, K., and Ohno, S. (2006). Lgl mediates apical domain disassembly by suppressing the PAR-3-aPKC-PAR-6 complex to orient apical membrane polarity. J. Cell Sci. *119*, 2107–2118.

Yamanaka, T., Horikoshi, Y., Sugiyama, Y., Ishiyama, C., Suzuki, A., Hirose, T., Iwamatsu, A., Shinohara, A., and Ohno, S. (2003). Mammalian Lgl forms a protein complex with PAR-6 and aPKC independently of PAR-3 to regulate epithelial cell polarity. Curr. Biol. *13*, 734–743.

Yang, M., Silverman, J., and Crawley, J. (2011). Automated three-chambered social approach task for mice. Curr. Protoc. Neurosci. *8*. Unit 8.26. https://doi.org/10.1002/0471142301.ns0826s56.

Zarnescu, D.C., Jin, P., Betschinger, J., Nakamoto, M., Wang, Y., Dockendorff, T.C., Feng, Y., Jongens, T.A., Sisson, J.C., Knoblich, J.A., et al. (2005). Fragile X protein functions with lgl and the par complex in flies and mice. Dev. Cell *8*, 43–52.

Zhu, J., Shang, Y., and Zhang, M. (2016). Mechanistic basis of MAGUK-organized complexes in synaptic development and signaling. Nat. Rev. Neurosci. *17*, 209–223.

ISCI, Volume *20*

Supplemental Information

Apical-Basal Polarity Signaling Components, Lgl1 and aPKCs, Control Glutamatergic Synapse Number and Function

John Scott, Sonal Thakar, Ye Mao, Huaping Qin, Helen Hejran, Su-Yee Lee, Ting Yu, Olga Klezovitch, Hongqiang Cheng, Yongxin Mu, Sourav Ghosh, Valeri Vasioukhin, and Yimin Zou

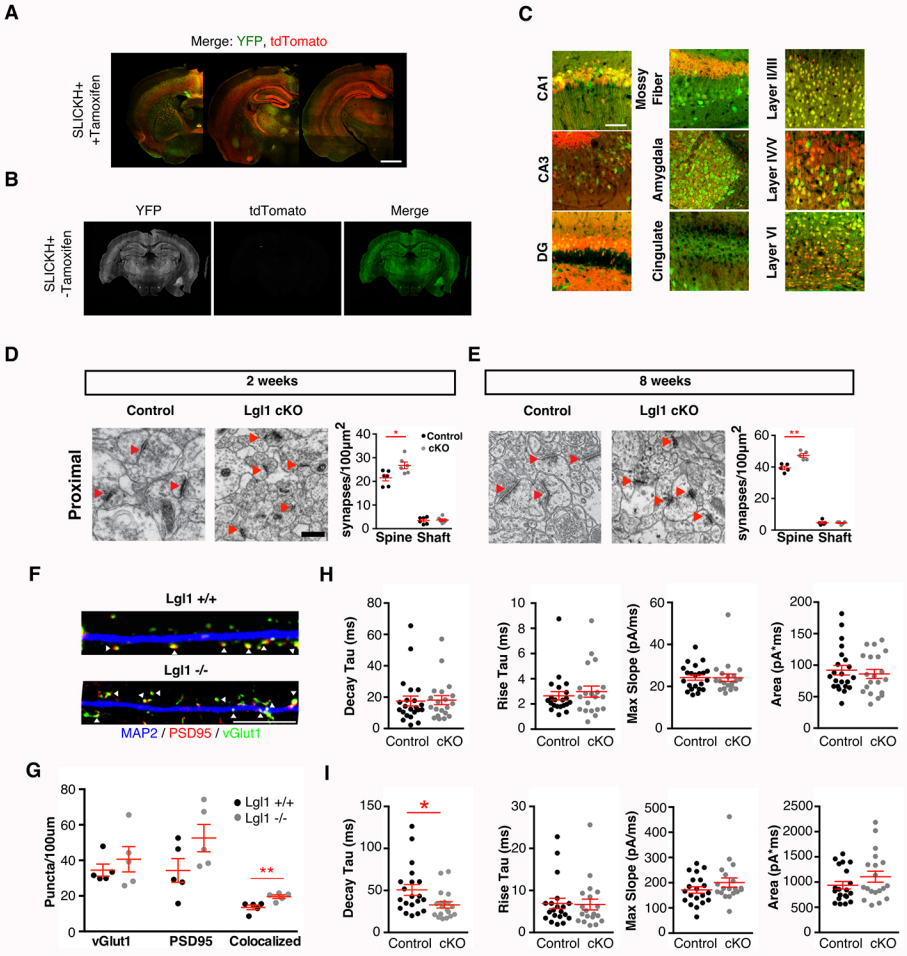

Figure S1 Related to Figure 1: Assessm ent of conditional deletion and characterization of current kinetics.

(**A**) Confocal images of brain slices from P14 mice injected with Tamoxifen at day P7 and P8 carrying SLICK-H shown by YFP (green) and *ROSA26-tdTomato* (red). Images show regions including the ventral hippocampal commissure and fimbria, dorsal hippocampus, and ventral hippocampus. Scale bar: 1mm. (**B**) Confocal images of brain slices of mice that were not injected with Tamoxifen, but carry SLICK-H and *ROSA26-tdTomato*. Scale bar: 1mm. (**C**) Images of brain regions expressing *Thy-1* cre in SLICK-H positive animals shown by YFP (green) and tdTomato (red). Scale bar: 100 μm. (**D**) EM micrographs taken 50μm from the CA1 pyramidal neuron layer in the Schaffer Collateral Region of P14 mice. Red arrows denote asymmetric synapses. Quantification of asymmetric synapse number: N = 6 control, 6 *Lgl1* cKO animals. (**E**) EM micrographs taken 50μm from the CA1 pyramidal neuron layer in the Schaffer Collateral Region of 8-week old mice. Red arrows denote asymmetric synapses. Quantification of asymmetric synapse number: N = 5 control, 5 *Lgl1* cKO animals. (**F**) Confocal images of dendrites (MAP2; blue) of neurons cultured for 14 DIV showing vGlut1 puncta (green) and PSD95 puncta (red). White arrowheads indicate colocalized pre- and post-synaptic puncta. Scale bar: 10 μm. (**G**) Quantification of puncta within ROIs including secondary dendrites of cultured hippocampal pyramidal neurons. N = 5 control, 5 KO embryos. (**H**) Quantification of kinetics of mEPSCs from slices from P13-15 control and *Lgl1* cKO mice. n = 22 control, 19 *Lgl1* cKO neurons. (**I**) Quantification of kinetics of mIPSCs from slices from P13-15 control and *Lgl1* cKO mice. n = 20 control, 19 *Lgl1* cKO neurons. *p<0.05; **p<0.01.

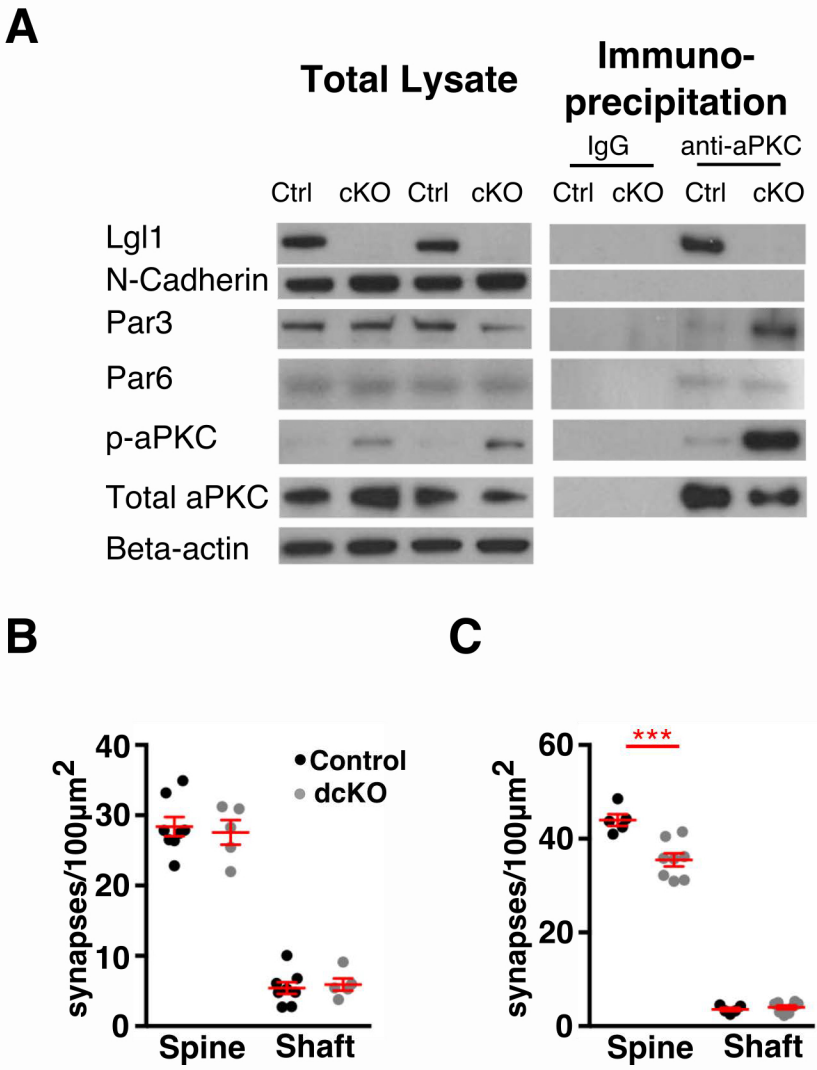

Figure S2 related to Figure 2: ***Atypical PKC*** **overactivation following** ***Lgl1*** **conditional deletion and synapse quantification in** ***aPKC dcKO*****.** (**A**) Western blots of total cell lysate and immunoprecipitation by anti-aPKC antibody from cultured neuronal progenitors treated with either AdGFP (Ctrl) or AdCre (cKO). (**B**) Quantification of asymmetric synapse number in the region of the Schaffer Collateral 50µm from the CA1 neuron layer in P14 control and *aPKC dcKO* animals. (**C**) Quantification of asymmetric synapse number in the region of the Schaffer Collateral 50µm from the CA1 neuron layer in 8-week old control and *aPKC dcKO* animals. ***p<0.001.

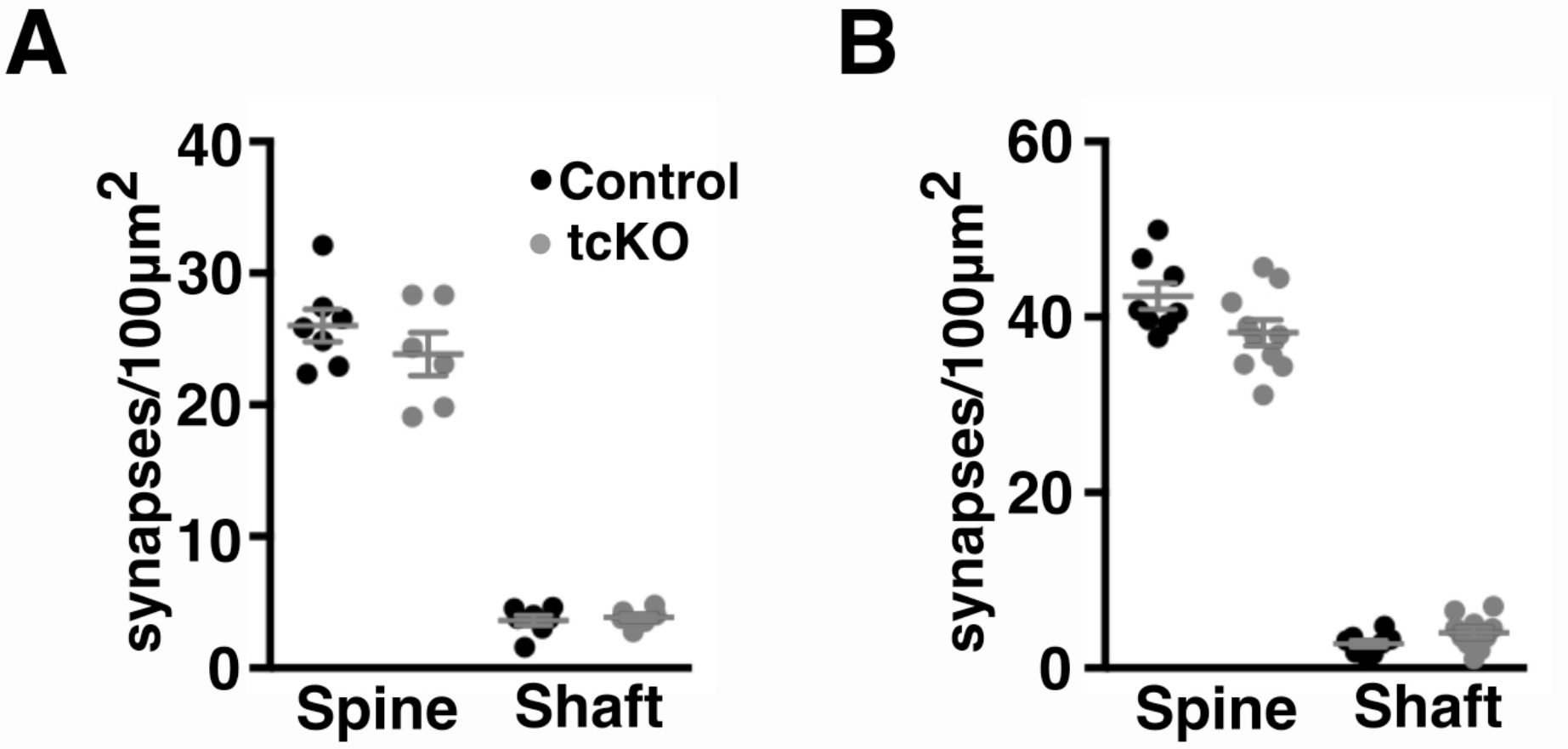

Figure S3 related to Figure 2: Synapse quantification in *Lgl1;PKCι/λ;PKCζ tcKO*. (**A**) Quantification of asymmetric synapse number in the region of the Schaffer Collateral 50µm from the CA1 neuron layer in P14 control and *Lgl1;PKCι/λ;PKCζ tcKO* animals. (**B**) Quantification of asymmetric synapse number in the region of the Schaffer Collateral 50µm from the CA1 neuron layer in 8-week old control and *Lgl1;PKCι/λ;PKCζ tcKO* animals.

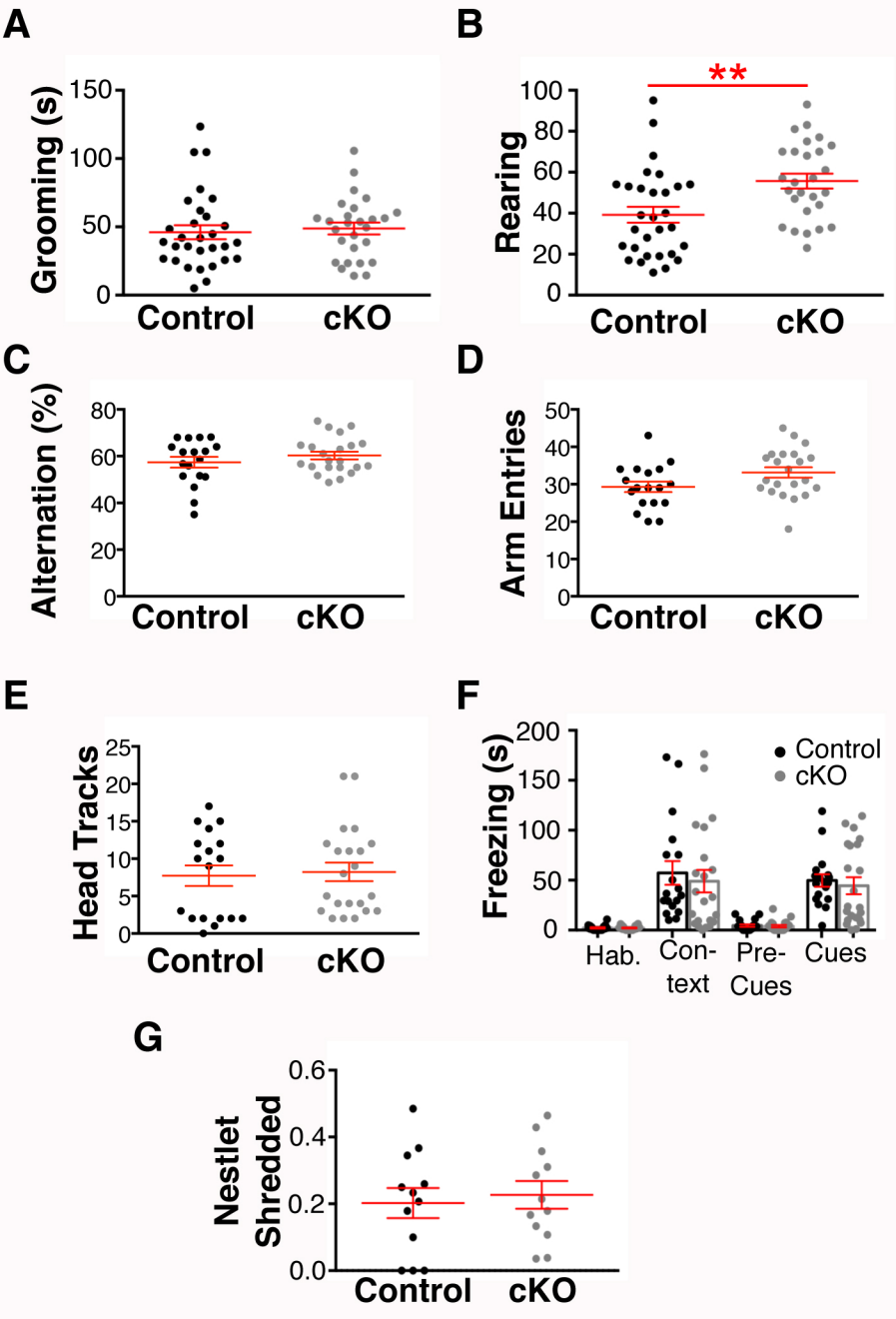

Figure S4 related to Figure 4: Additional behavioral characterization of *Lgl1* deletion at day P7. (**A**) Quantification of time spent self-grooming during the open field test. (**B**) Quantification of rearing counts during the open field test. (**C**) Quantification of spontaneous alternation in the Y-maze test following SLICK-H mediated *Lgl1* deletion at P7/P8. N = 18 control, 22 *Lgl1* cKO. (**D**) Total arm entries in the Y-maze test (not significant; p=0.0560) N = 18 control, 22 *Lgl1* cKO. (**E**) Number of 15-degree head movements during the optomotor response task. N = 18 control, 22 *Lgl1* cKO. (**F**) Quantification of the conditioned fear test following SLICK-H-mediated deletion of Lgl1. N = 18 control, 22 *Lgl1* cKO. (**G**) Quantification of nestlet-shredding activity following conditional *Lgl1* deletion at day P7. N = 12 control, 12 *Lgl1* cKO animals. **p<0.01.

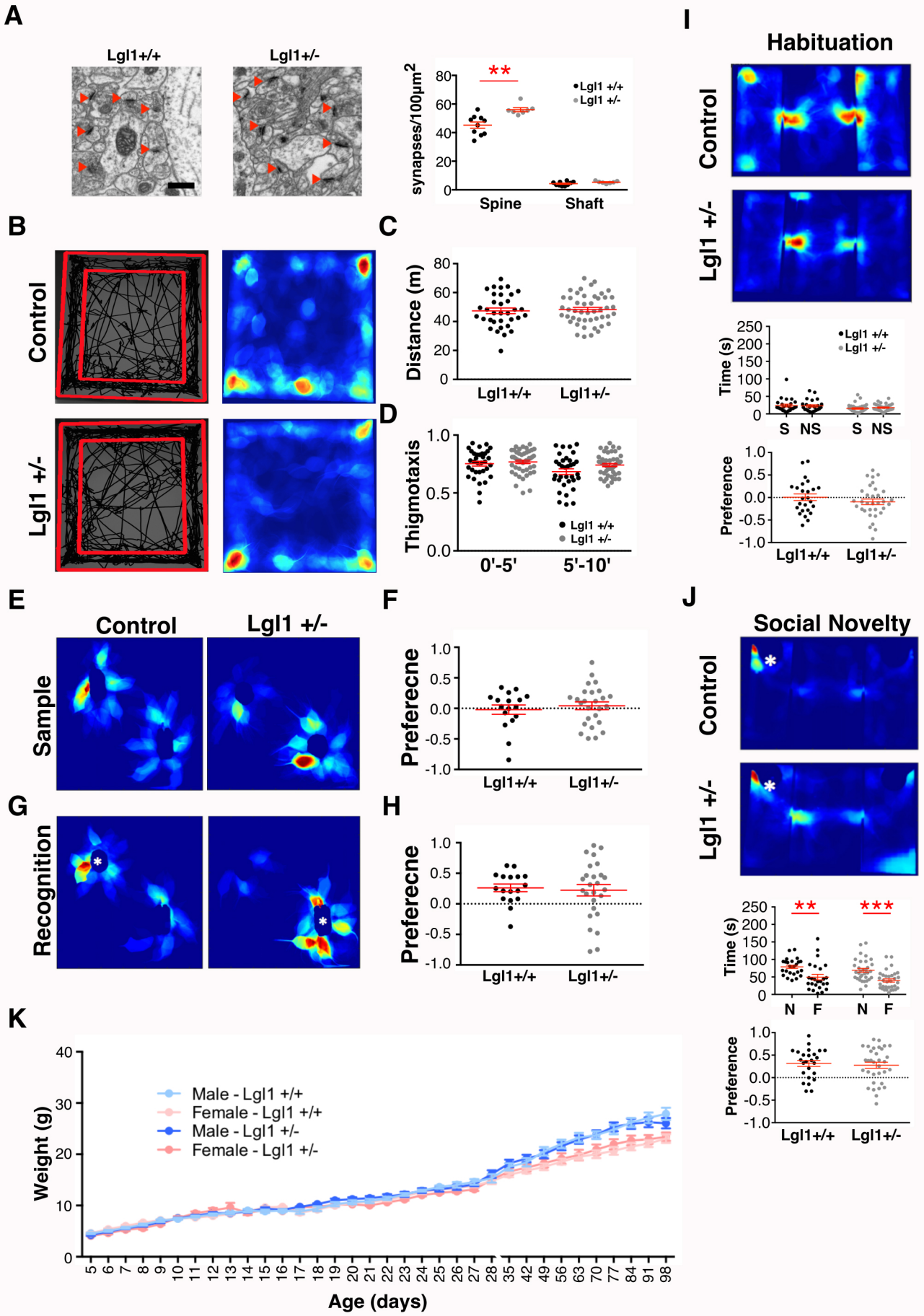

Figure S5 related to Figure 6: Partial preservation of behavioral phenotypes in *Lgl1*$^{+/-}$ mice. (**A**) Quantification of asymmetric synapse number in the region of the Schaffer Collateral 50µm from the CA1 neuron layer in P14 *Lgl1*$^{+/+}$ and *Lgl1*$^{+/-}$ animals. (**B**) Heat maps and Trajectories from *Lgl1*$^{+/+}$ and *Lgl1*$^{+/-}$ in the 10-minute open field (OF) test. (**C**) Quantification of distance travelled during the OF test. N = 34 control, 47 *Lgl1*$^{+/-}$ animals. (**D**) Quantification of Thigmotaxis for control (black) and Lgl1$^{+/-}$ (gray) mice. (**E**) Heat maps of interaction bouts from Control and *Lgl1* cKO from the sample phase of the novel object recognition (NOR) test. (**F**) Quantification of preference for objects during the sample phase. N = 17 control, 26 *Lgl1*$^{+/-}$ animals. (**G**) Heat maps of interaction bouts from the object recognition phase of the NOR test performed 2 minutes after the sample phase. White asterisk indicates location of the novel object. (**H**) Quantification of preference for objects. Positive value indicates preference for novel object. N = 17 control, 26 *Lgl1*$^{+/-}$ animals. (**I**) Heat maps and quantification from the habituation phase of the Social Interaction test. N = 25 control, 33 *Lgl1*$^{+/-}$ animals. (**J**) Heat maps and quantification from the social novelty phase of the SI test. N = 25 control, 33 *Lgl1*$^{+/-}$ animals. (**K**) Comparison of weight gain of *Lgl1*$^{+/+}$ and *Lgl1*$^{+/-}$ mice during development and early adulthood. Note discontinuous X-axis after P28 (N=9-15 male *Lgl1*$^{+/+}$, 9-15 male *Lgl1*$^{+/-}$, 8-15 female *Lgl1*$^{+/+}$, 9-14 female *Lgl1*$^{+/-}$).

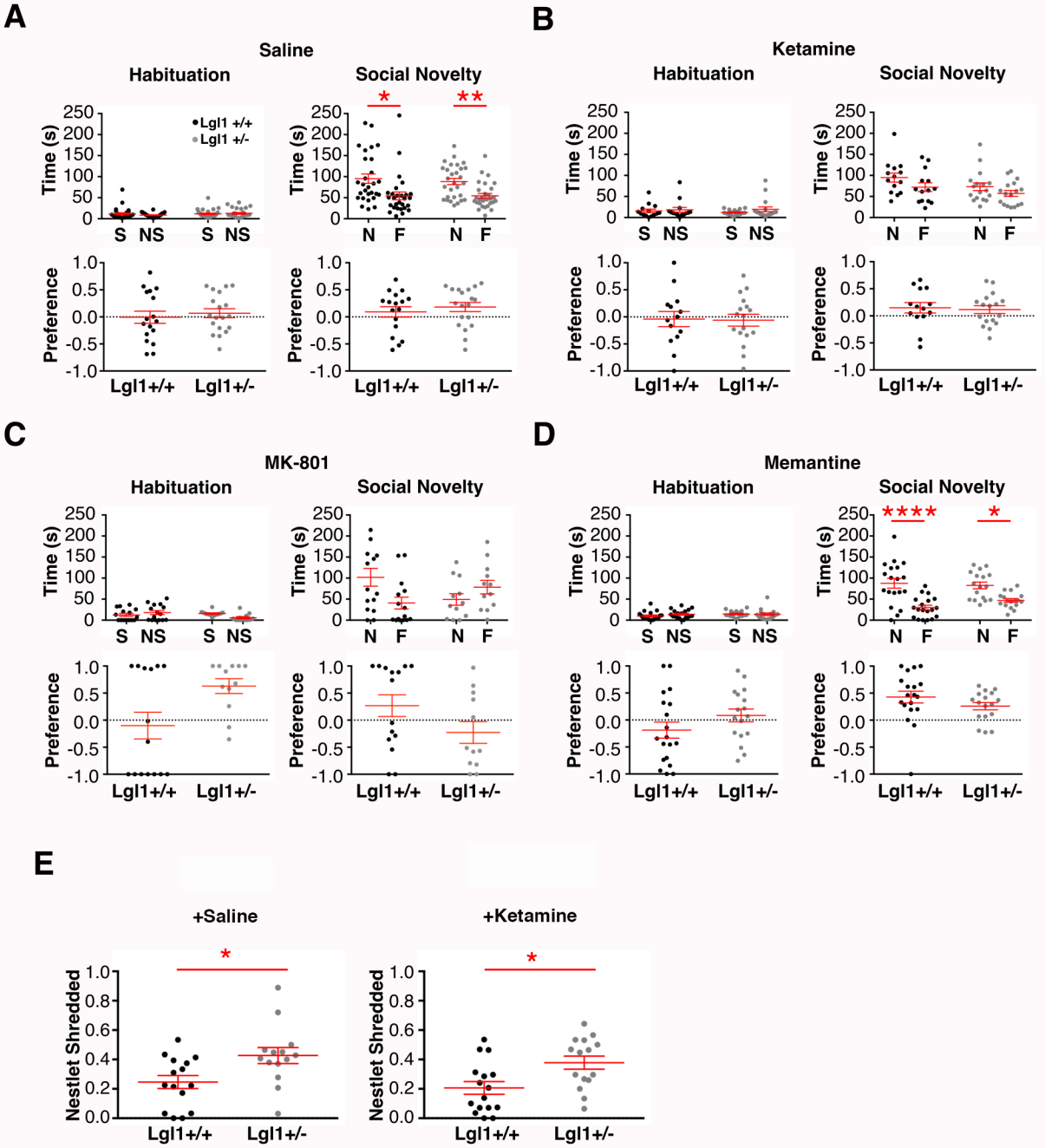

Figure S6 related to Figure 7: Additional phases of social interaction test in saline, ketamine, and MK-801 treated animals. (**A-D**) Quantification of interaction time and preference from the habituation and social novelty phases of the Social Interaction test following administration of the indicated solution. White asterisk indicates location of the novel mouse in the social novelty phase. N = (Saline) 27 *Lgl1*$^{+/+}$, 30 *Lgl1*$^{+/-}$ animals; (ketamine) 14 *Lgl1*$^{+/+}$, 17 *Lgl1*$^{+/-}$ animals; (MK-801) 13 *Lgl1*$^{+/+}$, 14 *Lgl1*$^{+/-}$ animals; (Memantine) 19 *Lgl1*$^{+/+}$, 17 *Lgl1*$^{+/-}$ animals. (**E**) Quantification of nestlet shredding activity following saline or ketamine injection. N = (Saline) 15 *Lgl1*$^{+/+}$, 14 *Lgl1*$^{+/-}$ animals; (ketamine) 15 *Lgl1*$^{+/+}$, 12 *Lgl1*$^{+/-}$ animals *p<0.05; **p<0.01; ****p<0.0001.

Methods

All animal procedures were performed in accordance with protocols approved by the Institutional Animal Care and Use Committee at Univesity of California, San Diego. Both male and female animals were analyzed in roughly equal numbers.

Electron Microscopy

Lgl cKO or *Lgl1*$^{+/-}$ and littermate control mice were anesthetized i. p. with a ketamine/xylazine cocktail, and perfused with modified Karnovsky's fixative (2.5% glutaraldehyde and 2% PFA in 0.15 M sodium cacodylate buffer, pH 7.4) at room temperature. After postfixation in the same solution overnight at 4 °C, whole brains were cut coronally (200 μm) with a vibratome. Sections were postfixed with 1% osmium tetroxide for 1 h on ice. Following en-block staining in 2% uranyl acetate in distilled water for 1-2 h, sections were dehydrated in a graded ethanol series and then treated twice in acetone for 10 min each. Sections were infiltrated in Durcupan resin (Sigma-Aldrich) and were embedded at 60 °C for 48 h. Ultrathin sections from CA1 region were cut and stained with uranyl acetate and Sato's lead. Image acquisition used a FEI Tecnai Spirit G2 Spirit BioTWIN transmission electron microscope equipped with an Eagle 4k HS digital camera (FEI, Hilsboro, OR). 10-15 fields from the distal stratum radiatum (150-200 μm from CA1 pyramidal cell bodies) and proximal stratum radiatum (40-50 μm from CA1 pyramidal cell bodies) were selected under 6800× magnification, and synapses were counted in each field. Synapses that displayed polyribosomes and/or actin bundles were determined to be on the dendritic shaft while synapses lacking those structures were determined to be on the dendritic spines. For ultrastructure analysis, asymmetric synapses from the distal stratum radiatum area were imaged at 18500× magnification. Only asymmetric synapses with a clearly recognized PSD and synaptic cleft were selected. The bouton area, cleft distance, reserve pool vesicles, docked vesicles, PSD width and PSD length were analyzed using Image J. Analysis of ultrastructure was done by experimenters blinded to animal genotype.

Hippocampal primary cell culture

Hippocampal neuron culture was performed as described below (Meffert et al., 2003). Glass coverslips were washed overnight in nitric acid and rinsed thoroughly and washed with 100% ethanol before being placed in a drying oven. The day before cell culturing, coverslips were coated with 80mg/mL Poly-D-Lysine (PDL) overnight at room temperature. Coverslips were washed and coated with 40mg/mL PDL with 2.5mg/mL Laminin for 3 hours at 37°C.
Brains from E18.5 pups were removed in L15 media and hippocampi were dissected and placed in individual tubes. Hippocampi were washed twice with Mg/Ca free sterile PBS (CellGro) and incubated with Trypsin/EDTA solution (0.25% Trypsin, 2.2mM EDTA) for 15 minutes at 37°C. Trypsin was neutralized by the addition of 10% vol/vol heat-inactivated horse serum (Life Technologies). Resulting solutions were pelleted and resuspended in Neurobasal medium supplemented with 2% B27 (Invitrogen), 5% fetal bovine serum (Invitrogen), penicillin/streptomycin (Cellgro), and Glutamax (Invitrogen) and washed twice. Cells density was determined and cells were plated at a density of $2.5x10^4$ cells/cm^2. Half of the growth

medium was exchanged every 3 days. Arabinofuranosyl Cytidine (Ara-C, 4 μM) was added at day 6 *in vitro* to prevent glial cell proliferation. Cultures were grown for 14 days at 37°C in a 5% carbon dioxide atmosphere.

Behavioral assays

For all behavioral assays, testing was performed during the light phase in a dimly lit room (<100 lux) with indirect lighting on the testing area unless otherwise noted. Both male and female animals were tested in behavior tests.

Open field test:
The open field test is performed in a plastic 40cm x 40cm acrylic box (Stoetling) with dark walls with a non-reflective base plate. Spatial cues are placed on one wall of the field. Mice are placed in the center of the field and allowed to explore freely for 10 minutes. Mice are scored for distance travelled, time in the inner and outer regions of the field, time spent self-grooming, rearing activity, and jumping activity. Outer region is defined as the region within 5 centimeters of the edge of the field. A 60-minute variant of the test was applied to the *Lgl1*$^{+/-}$ mice and littermate controls with all aspects of the testing area identical to the 10-minute test. Animals that performed the 10-minute test were not used for the 60-minute test in order to avoid effects of prior exposure to the testing apparatus.

Novel object recognition test:
The novel object recognition test was performed as described below (Antunes and Biala, 2012) immediately following a 10-minute exploration period in an empty apparatus. Animals are placed in a field containing two copies of a novel object and allowed to explore freely. After the sample phase, animals were removed from the field and the objects were replaced with one copy of the previously explored object and a novel object in the same positions in the field as during the sample phase. Animals were allowed to explore freely for 5 minutes. For scoring of interaction time, ROIs containing the target objects were selected in MATLAB. ROIs were selected by experimenters blinded to the animal genotypes or virus treatment.

Social interaction test:
The social interaction test was performed as previously described below (Yang et al., 2011). The sociability apparatus (Stoetling) has 3 20cm x 40 cm chambers and 2 target enclosures 7cm in diameter and 15cm tall. During testing, the apparatus was surrounded by opaque panels to prevent mice from seeing out of the apparatus.

Animals were placed in the center chamber of the 3-chambered sociability apparatus with the doors between chambers closed for 10 minutes to habituate to the testing conditions. The doors were removed and mice were allowed to explore the full field for 10 minutes. Non-littermate strain- and age-matched target mice from a separate cage were introduced during the social interaction phase of the test. For the social novelty phase, target mice from the social interaction phase were kept in the same location and a novel target mouse was introduced to the opposite chamber. For scoring of interaction time, ROIs containing the target mouse and

novel object were selected in MATLAB. ROIs were selected by experimenters blinded to the animal genotypes.

Scoring for distance travelled and thigmotaxis during the open field test, as well as time spent interacting with objects in the Novel Object Recognition test and time spent interacting with target mice and objects in the Social Interaction test was performed using Autotyping 15.04 in MATLAB 2014b (Patel et al., 2014)(MathWorks).

Nestlet shredding:
Mice were removed from their home cage and placed individually into a clean novel cage containing a weighed piece of cotton nesting material of approximately 2.8g. Mice were left in the cage for 60 minutes. At the end of the testing period, mice were returned to their home cage. Shredded material was separated from the undisturbed portion, which was weighed(Li et al., 2006).

Electrophysiology

For *Lgl1* cKOs and littermate controls at P13–15, mice were anesthetized by isofluorene. Mice were decapitated, and their brains were quickly removed and placed in ice-cold dissection buffer containing the following (in mM): 87 NaCl, 2.5 KCl, 1.25 NaH_2PO_4, 25 $NaHCO_3$, 20 glucose, 75 sucrose, 0.5 $CaCl_2$, and 7 $MgCl_2$, pH 7.35. Transverse hippocampal slices were cut in 300 μm-thick sections on a vibratome (Lieca VT1200). Slices were allowed to recover at 35°C for 20 min and then at room temperature for 1 to 6 hr in carbogenated ACSF, containing (in mM) 124 NaCl, 2.5 KCl, 24 $NaHCO_3$, 1.2 NaH_2PO_4, 2 $CaCl_2$, 2 $MgCl_2$ and 12.5 glucose, 5 HEPES pH 7.4. Individual slices were transferred to a recording chamber and then continuously perfused at a rate of 2–3 ml/min with ACSF containing 1 μM TTX (Tocris) and either 20 μM gabazine or 20 μM CNQX for mEPSC or mIPSC recordings, respectively. CA1 pyramidal cells were visualized by infrared differential interference microscopy.

For mEPSCs, whole-cell recordings were made using 3–5 MΩ pipettes filled with an internal solution that contained (in mM): 145 CH3O3SCs, 5 NaCl, 10 HEPES, 5 EGTA, 0.3 Na_2GTP and 4 MgATP, (pH was adjusted to 7.3 and osmolarity was maintained at 280–290 mOsm). For mIPSC recordings, whole-cell recordings were made using 3–5 MΩ pipettes filled with an internal solution that contained (in mM): 135 CsCl, 4 $MgCl_2$, 0.1 EGTA, 10 HEPES, 2 MgATP, 0.3 NaGTP, 10 Na_2Phosphocreatine (pH was adjusted to 7.3, and osmolarity was maintained at 280–290 mOsm).

Cells were voltage clamped at -70 mV. Recordings started after 5 minutes to allow for stabilization of the established whole-cell configuration. Signals were recorded with a 5× gain, low-pass filtered at 2 kHz and digitized at 5 kHz (Molecular Devices Axopatch 200B) with pCLAMP 10 software (Molecular Devices); analysis was performed with Clampfit (pCLAMP). The automatic detection was verified post hoc by visual inspection. Values are presented as mean ± SEM. Mann-Whitney U-statistic test was used to compare changes with the control.

For LTP induction, transvers hippocampus slices were harvested from 9-10-week-old mice. Slices were recovered for at least 1 hour before moving to recording chamber in aCSF (in mM): NaCl 119, KCl 2.5, NaH2PO4 1, NaHCO3 26.2, Glucose 11, MgCl2 1.3 and CaCl2 2.5 bubbled with 95% O2 and 5% CO2. Stimulus was given at 0.033 Hz to evoke field potential and the resistance of glass electrode was 1-2 MΩ with aCSF as internal solution. Input-Output were recorded by gradually increasing the strength of stimulus. After 30min stable baseline recording, LTP was induced by HFS or TBS. HFS was 100 pulses at 100 Hz. TBS contained four trains of theta bursts with 20 second intervals, each train had 10 burst with 0.2 interval.

For AMPA/NMDA ratio determination, a broken glass pipette was used as a stimulus electrode. The resistance of patch the clamp pipette was 3-5 MΩ. Internal solution: (in mM) CsMeSO4 115, CsCl 20, Na phosphocreatine 10, MgCl2 2.5, Na2ATP 4, Na3GTP 0.3, EGTA 0.6, HEPES 10 and QX-314-Cl 5. A cut was made between CA1 and CA3 to avoid epilepsy events. The position of stimulus electrode was gently adjusted to evoke a single peak EPSC. For AMPA current, holding potential was set at -70mV, and for NMDA current, holding potential changed to +40mV. We quantified NMDA current as the peak 100ms after stimulus artifact, where there is no AMPA current.

Biochemical fractionation

Subcellular fractionation was performed as previously described below (Cohen et al., 1977) with modifications. Forebrains from P14 wild type mice were homogenized to 10% (wt/vol) in ice cold 0.32M sucrose buffer containing 1mM MgCl2, 0.5mM CaCl2, 1mM NaHCO3 and protease inhibitors using 16 strokes with a glass dounce. The homogenates were spun at 710g for 30 min at 4C to pellet out nuclei and large debris. The supernatant was further centrifuged at 13800g for 10 min at 4C to get pellets (P2). P2 pellets were resuspended in the sucrose buffer and layered on top of a discontinuous sucrose gradient containing 1.0M and 1.4M sucrose in 4mM HEPES buffer pH 7.4. The gradient was centrifuged at 82500g for 1h at 4C. Synaptosomes were recovered from the cloudy band between 1.0M and 1.4M sucrose, resuspended in 1mM $NaHCO_3$ (1:9 vol/vol), and lysed by hypo osmotic shock using 3 strokes with a glass dounce. The lysates were then incubated with an equal volume of 0.32M sucrose buffer containing 1% Triton-X shaking at 4C for 15 min and spun at 82500g for 1h. The PSD fraction was obtained from the resulting pellet. The synaptic membrane fraction (SMF) was precipitated from the supernatant using the methanol/chloroform/H2O method(Wessel and Flügge, 1984). Both the PSD fraction and SMF were solubilized in 3% SDS for western blot analysis.

Western Blot

Protein samples were separated by polyacrylamide gel electrophoresis on 5% and 8% acrylamide gels and wet transferred to Immobilon membranes (Millipore). TBST with 5% non-fat dry milk (Apex) was used to block and primary antibody was diluted in blocking buffer for overnight incubation at 4°C. Blots were washed with TBST and incubated with HRP-conjugated secondary antibody for 2 hours at room temperature. Bands were visualized using West Pico

Chemiluminescent Substrate and exposed to film at intervals ranging from 30 seconds to 2 hours.

Antibodies

Primary antibodies were mouse anti-Lgl1 (gift of Valeri Vasioukhin), mouse anti-Lgl1 (Novus), Goat anti Vangl2 Antibody (N-13, Sant cruz, sc-46561), goat anti-JAM-C (R&D Systems), mouse anti-GAPDH (Abcam), and rabbit anti-GFP (Invitrogen), and chicken anti-MAP2 (Abcam). Secondary antibodies used in western blot were HRP-conjugated donkey anti-mouse, anti-goat, and anti-rabbit. For immunofluorescence, AF568-conjugated Donkey anti-Mouse (Invitrogen), AF488-conjugated Donkey anti-Chicken (Jackson Immunoresearch), AF488-conjugated Donkey anti-Rabbit (Invitrogen), AF647-conjugated Donkey anti-Rabbit (Invitrogen).

Cell filling and spine analysis

Mice were perfused, sectioned, and labeled with AlexaFluor Hydrazide as described below (Dumitriu et al., 2011). SLICK-H:*Lgl1*$^{flox/flox}$ pups were i. p. injected with tamoxifen at P7-8. At P14, pups were anesthetized with a ketamine/xylazine cocktail followed by transcardial perfusion with room temperature 4% PFA, postfixed for one hour in 4% PFA, vibratome sectioned at 100 μm, and then postfixed again for 10 minutes. AlexaFluor Hydrazide 555 (Invitrogen, 10 mM in 200 mM KCl) was injected into dendritic segments ionophoretically by filling the cell with fluorescent dye. Sections were briefly fixed for 15 minutes to preserve the fluorescent label. Immunolabeling with GFP antibody (Invitrogen) was used to confirm that the fluorescently filled dendrite is YFP+. 30-40 μm segments of CA1 oblique apical dendrites, which are located 100-200 μm from the CA1 pyramidal neuron cell bodies in the stratum radiatum, were analyzed. These spines represented the postsynaptic structures of the Schaffer collateral-CA1 synapses.

The maximum spine length and head width were measured manually with Image J (NIH) to characterize spine shape as described below (Bochner et al., 2014; Calfa et al., 2012; Harris et al., 1992; Tang et al., 2014; Vogel-Ciernia et al., 2013). Spines with heads equal to or less than the head width were categorized as “thin”, and those with heads greater than the neck width were categorized as “mushroom”. Spines without a neck that had a width longer than their lengths were termed “stubby”. Spines with one neck and a branch point resulting in 2 heads were termed “branched”. Protrusions not clearly seen or with lengths > 5 μm were excluded from analysis. Both image acquisition and morphometric analyses were done by experimenters blinded to the genotypes of the animals. Results were compared between littermates and then pooled by genotypes to assess the influence of prenatal care.

Tissue preparation

Animals were anesthetized i. p. with a ketamine/xylazine cocktail and perfused with ice-cold PBS followed by 4% Paraformaldehyde (PFA). Brains were post-fixed in 4% PFA overnight and moved to 30% sucrose until equilibrated. Frozen section embedded in OCT medium and Sucrose were sectioned at 40μm on a Leica CM 3050 S cryostat. Slides were stored at 4°C until immunostaining.

Immunostaining

For tissue sections, slides were rehydrated with 2 washed of PBS and permeabilized with PBS + 0.3% Triton X-100. Slides were blocked with 5% normal donkey serum for 2 hours at room temperature. Primary antibody was incubated at 4°C overnight and secondary antibody was incubated for 2 hours at room temperature. Slides were coverslip with Fluoromount-G (Southern Biotech) and stored at 4°C.

For cultured neurons, glass coverslips with primary cell cultures were washed with PBS and permeabilized with PBS + 0.1% Triton X-100. Coverslips were blocked with PBS containing 2% BSA, 2% Fetal Bovine Serum, and 0.1% Triton X-100. Primary antibody was incubated at 4°C overnight and secondary antibody was incubated for 2 hours at room temperature. Coverslips were inverted onto slides with Fluoromount-G (Southern Biotech) and stored at 4°C.

Statistical Analysis

Statistical analysis was performed using Prism 6 (GraphPad). Student's T-test with Welch's correction was used for comparison between control and Lgl1 mutant animals unless otherwise noted. One-way ANOVA with Tukey's multiple comparison test was used to test for statistical differences in interaction time during the social interaction test. Graphs of quantitative data present individual data points for animals with mean and standard error of the mean indicated unless otherwise noted. The Kolmogorov-Smirnov test was used to compare distribution of measurements of synaptic ultrastructure.

References:

Antunes, M., and Biala, G. (2012). The novel object recognition memory: neurobiology, test procedure, and its modifications. Cogn Process *13*, 93-110.

Bochner, D., Sapp, R., Adelson, J., Zhang, S., Lee, H., Djurisic, M., Syken, J., Dan, Y., and Shatz, C. (2014). Blocking PirB up-regulates spines and functional synapses to unlock visual cortical plasticity and facilitate recovery from amblyopia. Sci Transl Med *6*, 258ra140.

Calfa, G., Chapleau, C.A., Campbell, S., Inoue, T., Morse, S.J., Lubin, F.D., and Pozzo-Miller, L. (2012). HDAC activity is required for BDNF to increase quantal neurotransmitter release and dendritic spine density in CA1 pyramidal neurons. Hippocampus *22*, 1493-1500.

Cohen, R., Blomberg, F., Berzins, K., and Siekevitz, P. (1977). The structure of postsynaptic densities isolated from dog cerebral cortex: I. overall morphology and protein composition. Journal of Cell Biology *74*, 181-203.

Dumitriu, D., Rodriguez, A., and Morrison, J. (2011). High-throughput, detailed, cell-specific neuroanatomy of dendritic spines using microinjection and confocal microscopy. Nature Protocols *6*, 1391-1411.

Harris, K.M., Jensen, F.E., and Tsao, B. (1992). Three-dimensional structure of dendritic spines and synapses in rat hippocampus (CA1) at postnatal day 15 and adult ages: implications for the maturation of synaptic physiology and long-term potentiation. Journal of Neuroscience *12*, 2685-2705.

Li, X., Morrow, D., and Witkin, J. (2006). Decreases in nestlet shredding of mice by serotonin uptake inhibitors: Comparison with marble burying. Life Sci *78*, 1933-1939.

Meffert, M., Chang, J., Wiltgen, B., Fanselow, M., and Baltimore, D. (2003). NF-kappa B functions in synaptic signaling and behavior. Nature Neuroscience *6*.

Patel, T.P., Gullotti, D.M., Hernandez, P., O'Brien, W.T., Capehart, B.P., Morrison, B., Bass, C., Eberwine, J.E., Abel, T., and Meaney, D.F. (2014). An open-source toolbox for automated phenotyping of mice in behavioral tasks. Frontiers in Behavioral Neuroscience *8*, 1-16.

Tang, G., Gudsnuk, K., Kuo, S., Cotrina, M., Rosoklija, G., Sosunov, A., Sonders, M., Kanter, E., Castagna, C., Yamamoto, A.*, et al.* (2014). Loss of mTOR-dependent macroautophagy causes autistic-like synaptic pruning deficits. Neuron *83*, 1131-1143.

Vogel-Ciernia, A., Matheos, D., Barrett, R., Kramár, E., Azzawi, S., Chen, Y., Magnan, C., Zeller, M., Sylvain, A., Haettig, J.*, et al.* (2013). The neuron-specific chromatin regulatory subunit BAF53b is necessary for synaptic plasticity and memory. Nat Neurosci *16*, 552-561.

Wessel, D., and Flügge, U. (1984). A method for the quantitative recovery of protein in dilute solution in the presence of detergents and lipids. Anal Biochem *138*, 141-143.

Yang, M., Silverman, J., and Crawley, J. (2011). Automated Three-Chambered Social Approach Task for Mice. Curr Protoc Neurosci *8*, Unit 8.26.